Theor. Comput. Fluid Dyn. (2018) 32: 109–136
https://doi.org/10.1007/s00162-017-0442-0

ORIGINAL ARTICLE

Kiran Ramesh · Kenneth Granlund · Michael V. Ol · Ashok Gopalarathnam · Jack R. Edwards

Leading-edge flow criticality as a governing factor in leading-edge vortex initiation in unsteady airfoil flows

Received: 10 October 2016 / Accepted: 26 July 2017 / Published online: 14 August 2017

Abstract A leading-edge suction parameter (LESP) that is derived from potential flow theory as a measure of suction at the airfoil leading edge is used to study initiation of leading-edge vortex (LEV) formation in this article. The LESP hypothesis is presented, which states that LEV formation in unsteady flows for specified airfoil shape and Reynolds number occurs at a critical constant value of LESP, regardless of motion kinematics. This hypothesis is tested and validated against a large set of data from CFD and experimental studies of flows with LEV formation. The hypothesis is seen to hold except in cases with slow-rate kinematics which evince significant trailing-edge separation (which refers here to separation leading to reversed flow on the aft portion of the upper surface), thereby establishing the envelope of validity. The implication is that the critical LESP value for an airfoil–Reynolds number combination may be calibrated using CFD or experiment for just one motion and then employed to predict LEV initiation for any other (fast-rate) motion. It is also shown that the LESP concept may be used in an inverse mode to generate motion kinematics that would either prevent LEV formation or trigger the same as per aerodynamic requirements.

Keywords LESP · LEV · Vortex dynamics · Unsteady aerodynamics · Low Reynolds number · Flow separation

List of symbols

α	Angle between the airfoil and inertial horizontal
$\dot{\alpha}$	Pitch rate
$\dot{h}$	Plunge rate
η	Variation of camber along airfoil
γ	Chordwise distribution of bound vorticity on airfoil
Γ_b	Bound circulation of airfoil at time t
Γ_{tev_m}	Strength of mth wake/trailing-edge vortex

Communicated by Jeff D. Eldredge.

K. Ramesh (✉)
Aerospace Sciences Division, School of Engineering, University of Glasgow, Glasgow G12 8QQ, UK
E-mail: kiran.ramesh@glasgow.ac.uk

K. Granlund · A. Gopalarathnam · J. R. Edwards
Department of Mechanical and Aerospace Engineering, North Carolina State University, Raleigh, NC 27695-7910, USA

M. V. Ol
U.S. Air Force Research Laboratory, Air Vehicles Directorate AFRL/RBAL, Bldg. 45, 2130 8th St., WPAFB, Dayton, OH 45433-7542, USA

ω	Angular frequency
ϕ	Velocity potential
ϕ_{B}	Velocity potential from bound circulation
ϕ_{tev}	Velocity potential from trailing-edge vorticity (wake circulation)
θ	Variable of transformation of chordwise distance
$A_0, A_1, A_2 \ldots$	Fourier coefficients
$Bxyz$	Body frame
c	Airfoil chord
C_{f}	Skin friction coefficient
C_{p}	Pressure coefficient
h	Plunge displacement in the inertial Z direction
$K = \dot{\alpha}c/2U$	Reduced frequency (ramp)
$k = \omega c/2U$	Reduced frequency (sinusoidal)
LESP	Leading-edge suction parameter
$\mathrm{LESP}_{\mathrm{crit}}$	Critical value of LESP corresponding to LEV initiation
$OXYZ$	Inertial frame
Re	Reynolds number
t	Time
t^*	Nondimensional time $= tU/c$
U	Freestream velocity
W	Local downwash
x_{p}	Pivot location on the airfoil from 0 to c

1 Introduction

Low-Reynolds-number flows at low speeds and small scales, despite being incompressible and nonthermodynamic, are rife with complexity owing to the effects of viscosity and flow separation [49]. Much research on this topic in the twenty-first century has been driven by interest in micro-air vehicle (MAV) design, a problem at the interface between low *Re* fluid mechanics and flight vehicle engineering [48,49]. The design problem in this regime has been driven by seeking bio-inspiration from insects which employ flapping flight at high dimensionless rates of motion (reduced frequencies) to achieve remarkable flying prowess. It has been shown that the single most important aerodynamic phenomenon largely responsible for the success of flapping flight at low Reynolds numbers is the leading-edge vortex (LEV) [16,21,22,65]. The conditions under which such LEVs develop on rounded-leading-edge airfoils form the subject of this study and are investigated with a large set of unsteady test cases using experiments, computations, and theoretical methods. Two-dimensional problems without additional complexity involving spanwise flow and wingtip vortices are considered here and serve as a starting point for more complex investigations.

LEV formation is initiated by reversed flow at the airfoil surface in the vicinity of the leading edge, followed by the formation of a free shear layer. The free shear layer then builds up into a vortex, which traverses the airfoil chord and convects into the wake [40]. Research contributions on LEV formation have largely arisen from the rotorcraft community and the more recent low-*Re*/MAV community.

Dynamic stall encountered in helicopters has prompted the rotorcraft research community to study the onset and effects of LEVs [41,44]. Dynamic stall refers to unsteady separation and stall phenomenon on airfoils that execute time-dependent motion, in which the effective angle of attack exceeds the static stall angle [43,45]. These flows are characterized by a delayed onset of flow separation/stall, followed by the shedding of a vortex from the leading edge of the airfoil which traverses the airfoil chord [40, chap. 9]. Although this vortex enhances the lift when it stays over the surface of the airfoil, it also creates large nose-down pitching moments and flow separation over the entire airfoil when it convects off the trailing edge. Hence dynamic stall can lead to violent vibrations and dangerously high airloads, resulting in material fatigue and structural failure. A good review of experimental and numerical approaches toward understanding and predicting dynamic stall in given by Carr [7] and Carr et al. [8]. Dynamics stall in rotorcraft is necessarily associated with relatively low reduced frequencies of motion (typically $k = \omega c/2U < 0.5$).

Research on low *Re* unsteady aerodynamics of interest to insect flight and MAV design, typically focuses on higher reduced frequencies of motion than those relevant to rotorcraft flight. Here, the LEVs that enable high lift and highly maneuverable flight are seen to form with insignificant flow separation over the rest of the

airfoil surface. In this category, McGowan et al. [46] and Ol et al. [50] have analyzed the forces and flowfields for unsteady motions with LEVs over a broad parameter space using both experimental and computational methods. High-fidelity simulations of moving and flexible airfoils to characterize unsteady phenomena at low Reynolds numbers have been performed by Visbal et al. [70]. Garmann and Visbal [25] and Granlund et al. [29] have investigated vortex structures on pitching flat plates in detail through computational and experimental methods, respectively. Pitt and Babinsky [55], Baik et al [3], and Rival et al. [61] have studied the effects of leading edge vortices using experimental techniques. Widmann and Tropea [75] have recently used experiments to investigate mechanisms responsible for the formation and detachment of LEVs. Other recent contributions characterizing 3D vortical structures on unsteady plates using high-fidelity simulations and experiments include those by Visbal et al. [72], Devoria and Ringuette [15], Carr et al. [9], Jones and Babinsky [32,33], Panah et al. [53], and Bos et al. [5].

Aside from experimental and computational methods, low-order models based on theoretical formulations also provide unique insight into the underlying physics in unsteady vortex-dominated flows. Since closed-form solutions from theory are incapable of capturing nonlinear effects, they may be suitably augmented with numerical procedures to expand their range of applicability. Wang and Eldredge [74], Hemati et al. [30], Taha et al. [67], and Brunton et al. [6] have developed such phenomenologically augmented theoretical methods. These, and the model developed in this research, are largely founded on the results from early pioneering theoretical and experimental research in unsteady aerodynamics including Theodorsen [69], Wagner [73], Pinkerton [54], Jones [35], and Woods [76], reviewed in Sears [63]. The class of phenomenologically augmented inviscid/theoretical methods allows one to study in more depth the influence of various individual parameters on the unsteady flow physics.

A new theoretical method based on the unsteady thin-airfoil theory developed by Katz and Plotkin [38], accounting for large amplitudes of motion and nonplanar wakes was developed by the Ramesh et al. [57] and applied to a ramp-hold-return pitching maneuver. The results from this model were compared against those from Reynolds-averaged Navier–Stokes computational fluid dynamics (CFD) and experimental (water tunnel) methods. By accounting for the effects of nonplanar wakes, large amplitudes, and high rates of motion, the results from the model of Ramesh et al. matched those from CFD and experiment reasonably well as long as the flow at the leading edge was attached. In LEV-dominated regions of the flow, however, the comparison with CFD and experiment was poor. It was hence shown that low-order modeling in the low *Re* unsteady regime can only be successful if a model for LEV formation and shedding is considered. Following this, Ramesh et al. developed the leading-edge suction parameter (LESP), a time-varying parameter, easily determined using unsteady airfoil theories, that provides a measure of the suction force developed at the airfoil leading edge. They demonstrated that for flows around a given airfoil operating at a given Reynolds number, LEV shedding is always initiated at a critical value of the LESP [59] and is independent of motion kinematics, provided that LEV formation is not preceded by significant trailing-edge separation. Additionally, Ramesh et al. [58] developed a novel low-order numerical solver, called LDVM, for 2D low *Re* unsteady flows, using the LESP to predict and modulate LEV shedding. In the LDVM, when the instantaneous value of LESP exceeds a pre-determined critical value, LEV shedding is modeled by shedding a discrete vortex at each time step of the numerical method. The strength of the discrete vortex is determined so as to keep the LESP at the critical value during the LEV shedding. In this research, we focus less on the low-order modeling aspects and more on the conditions under which LEV formation is initiated. Therefore, the low-order method used in the current work is an inviscid unsteady thin-airfoil theory with no discrete vortex shedding from the leading edge. We study the LESP concept in more detail using a large set of experimental and CFD studies involving LEV formation, spanning a broad range of relevant parameters, with an aim toward establishing the envelope of applicability of the LESP criterion and also to isolate the effect of various parameters on LEV formation.

It has been known for several decades, especially among the dynamic stall community, that onset of separation at the leading edge is governed by the criticality of flow properties at the leading edge. Evans and Mort [23] showed that leading-edge separation is directly related to the strong adverse pressure gradient generated at the leading edge. Beddoes [4] has shown an equivalent correspondence between leading-edge flow separation and flow velocity at the leading edge. Jones and Platzer[34] have studied the onset of laminar separation at the leading edge for a pitching NACA 0012 airfoil as an indication of the initiation of dynamic stall. They showed that the angle of attack at which the laminar separation first occurs increases with pitch rate. This result was shown to be in qualitative agreement with experiments of Chandrasekhara et al.[11]. More interestingly, at the angle of attack corresponding to the first occurrence of laminar separation at the leading edge, the leading-edge flows (pressure distributions, pressure gradient distributions, and locations of stagnation and laminar separation points) were found to be invariant with pitch rate [19]. The LESP criterion was inspired

by these results, with an objective to predict LEV formation using a flow quantity from inviscid theory and serve as a theoretical parameter to modulate leading-edge vortex shedding in low *Re* unsteady flows.

In Sect. 2, the large-angle unsteady thin-airfoil theory used to derive the LESP is briefly reviewed, and the LESP hypothesis is presented. Section 3 presents the computational and experimental methods used in this work. In Sect. 4, the test cases chosen for the experimental and numerical campaign in this paper are listed and discussed, and the results presented. The regimes where the LESP criterion holds valid are identified, and the reasoning is presented. The relative significance and influence of various parameters on the initiation of LEV formation are studied. Furthermore, using the observation that LEV formation occurs only when the LESP reaches the critical value, it is shown that the motion kinematics can be designed to either avoid or intentionally trigger LEV formation by tailoring the LESP variation.

2 Theoretical approach

This section describes the theoretical methods employed in this research and the LESP hypothesis. The interested reader may refer to references [57] and [58] for greater detail.

2.1 Large-angle unsteady thin-airfoil theory

The large-angle unsteady thin airfoil builds on the time-stepping approach given by Katz and Plotkin [38]. It aims to eliminate the traditional small-angle assumptions in thin-airfoil theory which are invalid in high amplitude, high frequency or vortex-dominated flows, such as those considered in this research. In Fig. 1a, the inertial frame is given by $OXYZ$ and the body frame, attached to the moving airfoil, by $Bxyz$. At time $t = 0$, the two frames coincide, and at time $t > 0$, the body frame moves toward the left of the page along any prescribed time-varying path (given by pitch and plunge motions). At each time-step, a discrete trailing-edge vortex is shed from the trailing edge.

Analogous to classical thin-airfoil theory, the vorticity distribution over the airfoil, $\gamma(x)$, is taken to be a Fourier series,

$$\gamma(\theta, t) = 2U \left[A_0(t) \frac{1 + \cos\theta}{\sin\theta} + \sum_{n=1}^{\infty} A_n(t) \sin(n\theta) \right] \tag{1}$$

where θ is a variable of transformation related to the chordwise coordinate x as,

$$x = \frac{c}{2}(1 - \cos\theta) \tag{2}$$

in which $A_0(t)$, $A_1(t), \ldots, A_n(t)$ are the time-dependent Fourier coefficients, c is the airfoil chord, and U is the component of the airfoil's velocity in the negative X direction. The Kutta condition (zero vorticity at the trailing-edge) is enforced implicitly through the form of the Fourier series. The Fourier coefficients are determined as a function of the instantaneous downwash on the airfoil by enforcing the boundary condition that the flow must remain tangential to the airfoil surface.

$$A_0(t) = -\frac{1}{\pi} \int_0^{\pi} \frac{W(x,t)}{U} \mathrm{d}\theta \tag{3}$$

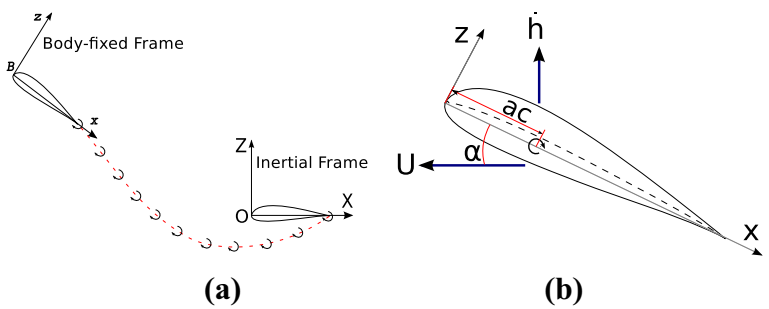

Fig. 1 **a** Illustration of the time-stepping method in large-angle unsteady thin-airfoil theory, **b** Airfoil velocities (positive as shown) and pivot location

$$A_n(t) = \frac{2}{\pi}\int_0^{\pi} \frac{W(x,t)}{U}\cos n\theta \mathrm{d}\theta \tag{4}$$

The downwash on the airfoil surface, $W(x,t)$, is calculated from components of motion kinematics, depicted in Fig. 1b, and induced velocities from vortices in the flowfield.

$$\begin{aligned} W(x,t) \equiv \frac{\partial \phi_{\mathrm{B}}}{\partial z} = \frac{\partial \eta}{\partial x}\left(U\cos\alpha + \dot{h}\sin\alpha + \frac{\partial \phi_{\mathrm{tev}}}{\partial x}\right) - U\sin\alpha - \dot{\alpha}(x-ac) \\ + \dot{h}\cos\alpha - \frac{\partial \phi_{\mathrm{tev}}}{\partial z} \end{aligned} \tag{5}$$

where ϕ_B and ϕ_{tev} are the velocity potentials associated with bound and trailing-edge vorticity, $\eta(x)$ is the camber distribution on the airfoil, $\frac{\partial \phi_{\mathrm{tev}}}{\partial x}$ and $\frac{\partial \phi_{\mathrm{tev}}}{\partial z}$ are velocities induced tangential and normal to the chord by trailing edge discrete vortices. The motion parameters include the plunge velocity in the Z direction, $\dot{h}$, and the pitch angle of the chord with respect to the X direction, α. Trailing-edge vortices are shed at every time step as mentioned earlier, and their strengths are calculated iteratively such that Kelvin's circulation condition is enforced.

$$\Gamma_{\mathrm{B}}(t) + \sum_{m=1}^{N_{\mathrm{tev}}} \Gamma_{\mathrm{tev}_m} = 0 \tag{6}$$

where Γ_{B} is the bound circulation calculated by integrating the chordwise distribution of bound vorticity over the airfoil chord:

$$\Gamma_{\mathrm{B}} = Uc\pi\left[A_0(t) + \frac{A_1(t)}{2}\right] \tag{7}$$

2.1.1 Leading-edge suction parameter (LESP)

In thin-airfoil theory, the airfoil thickness and hence the leading-edge radius is zero. This requires the flow to turn 180° around the leading edge (Fig. 2), giving rise to a theoretically infinite flow velocity at the leading edge, V_{LE}, of a thin airfoil. From Garrick [26] and von Kármán and Burgers [36], we have that the form of this theoretically infinite velocity is given by,

$$V_{\mathrm{LE}}(t) = \lim_{x\to \mathrm{LE}} \frac{S}{\sqrt{x}} \tag{8}$$

where S is a measure of the suction at the leading edge and is given by,

$$S = \lim_{x\to \mathrm{LE}} \frac{1}{2}\gamma(x,t)\sqrt{x} \tag{9}$$

Since $\gamma(x,t)$ is infinite in order of $1/\sqrt{x}$ at the leading edge, the value of S is finite. Evaluating using the current formulation,

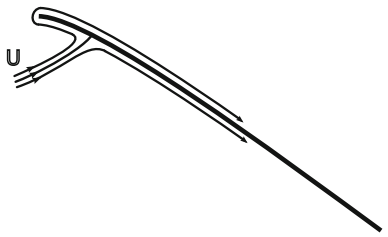

Fig. 2 Depiction of flow around a thin airfoil's leading edge

$$S = \sqrt{c}U A_0(t) \tag{10}$$

Because the LESP is a nondimensional measure of the suction at the leading edge, S, for given values of c and U, we may simply equate it to the A_0 value as,

$$\text{LESP}(t) = A_0(t) \tag{11}$$

As discussed in Katz [37], real airfoils have rounded leading edges which can support some suction even when the stagnation point is away from the leading edge. The amount of suction that can be supported is dependent on the airfoil shape and Reynolds number of operation. Since the LESP (the A_0 value) is a measure of the suction/velocity at the leading edge, it is a logical choice to develop a correlation for initiation of LEV formation based on the LESP.

Using inviscid parameters to predict trends in viscous behavior has long been employed by the aerodynamics research community. An example is Polhamus' leading-edge suction analogy [56], in which the leading-edge suction force associated with potential flow about the airfoil is simply rotated by 90° to predict the vortex lift on delta wings. To clarify, the current LESP concept is not related to Polhamus' analogy either in formulation or in objectives. The A_0 term has also been previously used to develop useful correlations in steady aerodynamic theory. For example, the ideal lift coefficient of a laminar-flow airfoil in steady flow, which usually falls close to the middle of the drag bucket, corresponds to the lift coefficient at which the A_0 coefficient is zero [1,68]; this idea can be used to estimate the C_l-shift in the drag bucket due to a trailing-edge cruise flap [42]. Morris and Rusak [47] have studied leading-edge stall on 2D, stationary, thin airfoils using matched asymptotic theory and shown that leading-edge stall is related to a critical A_0 value. It follows, therefore, that a critical value of A_0 would correspond to initiation of LEV formation in unsteady flow.

2.2 LESP hypothesis

The statement of the LESP hypothesis is that, for a given airfoil and Reynolds number combination, the critical LESP, which is the LESP value corresponding to LEV initiation, is independent of motion kinematics. This hypothesis is based, in part, on the argument that, for a rounded leading edge of an airfoil that is operating at a given chord Reynolds number, attached flow around the leading edge is supported so long as leading-edge suction is below a critical value. When this critical value is exceeded, the flow at the leading edge will separate, resulting in the shedding of vorticity from the leading edge. Because the LESP is a motion-independent, nondimensional measure of the leading-edge suction, it should be a good predictor of LEV initiation for any motion. The major benefit of this hypothesis being true is that the critical LESP can be determined for one motion from CFD or experiment and can then be used for prediction of LEV initiation for any other motion.

The major caveat to the hypothesis is that the LESP, in the current theoretical approach, is determined using inviscid theory (unsteady thin-airfoil theory), in which the flow over the upper surface is assumed to be attached. Thus, in situations characterized by trailing-edge flow separation on the airfoils, this inviscid LESP is unlikely to be a true measure of the leading-edge suction. Trailing-edge separation, here, refers to flow separation off the upper surface of the airfoil resulting in reversed flow over the aft portion of the upper surface similar to that seen in trailing-edge stall on airfoils. By trailing-edge separation, we do not refer to vortex shedding in unsteady flow from the sharp trailing edge of an airfoil. To further develop this idea, consider two situations in which a given airfoil operating at a given Reynolds number has the same LESP value. These two situations could be time instants in two different motions at which the LESP is the same. If one situation corresponds to negligible trailing-edge flow separation and the other has significant extent of flow separation, then the leading-edge suction in the two situations will not be the same even though the inviscid LESP values are the same. Thus, it is clear that the LESP hypothesis is likely to be true only as long as the LEV initiation is not preceded by significant trailing-edge separation, a situation that is observed for high values of nondimensional pitch rate. For low nondimensional pitch rates, such as those commonly associated with helicopter dynamic stall, the current LESP hypothesis is unlikely to be applicable. More specifically, the critical value of LESP derived from high-rate motions is unlikely to correctly predict LEV initiation for low-rate motions.

The objective of the current research is to use a large range of motion kinematics for a given airfoil and Reynolds number to test the LESP hypothesis, and assess the bounds of validity using several motions including some that evince trailing-edge flow separation prior to LEV formation.

3 Computational and experimental methods

The CFD calculations were performed using NCSU's REACTMB-INS code, which solves the time-dependent incompressible Navier–Stokes equations using a finite-volume method. The governing equations are written in arbitrary Lagrangian/Eulerian (ALE) form, which enables the motion of a body-fitted computational mesh in accord with prescribed rate laws. An implicit, dual time-stepping artificial compressibility method is used for time advancement, with sub-iterations performed each physical time-step to adjust the flow to the new position of the body and to converge the continuity equation. Spatial discretization of the inviscid fluxes uses a low-diffusion flux-splitting method valid in the incompressible limit [10]. The Spalart–Allmaras model [66], as implemented by Edwards and Chandra [18], is used for turbulence closure. The cases studied, however, are at low Reynolds numbers, and turbulence model effects are generally confined to the wake. The computations were performed on a 2-D body-fitted mesh containing 92,400 cells. REACTMB-INS has been used for a wide variety of CFD problems, including unsteady aerodynamics [52,57], two-phase flows [10], human-induced contaminant transport [12,13], and moving-body flows [14].

The experiments were performed at the U.S. Air Force Research Laboratory's Horizontal Free-surface Water Tunnel, which is fitted with a three-degree-of-freedom electric motion rig enabling independent control of pitch, plunge and surge (streamwise-aligned translation). More detail on the rig operation is given in refs. [50] and [28], while the facility is discussed in ref. [51]. The flowfield is visualized by planar laser fluorescence. A high concentration of Rhodamine 6G in water is injected at the leading and trailing edges at 3/4-span locations by a positive-displacement pump at a prescribed volumetric infusion rate, via a 0.5-mm-diameter internal rigid line, as documented by Ol et al. [50]. The dye is illuminated by an Nd:YLF 527 nm pulsed laser sheet of 1.5 mm thickness at 50 Hz, and images are recorded with a PCO DiMax high-speed camera through a Nikon PC-E 45 mm micro-lens. An orange Wratten #21 filter removes the incident and reflected laser light since the dye fluorescence wavelength is 566 nm. Force data are recorded from an ATI Nano-25 IP68 6-component integral load cell, oriented with its cylindrical axis normal to the pitch–plunge–surge plane. Experimental force data are ensemble-averaged over ten repetitions of the motion.

4 Study of LEV initiation in low-Reynolds-number flows

Trends in LEV initiation for various motion kinematics and the validity of the LESP hypothesis are analyzed in this section using data sets from CFD and experiments. An SD7003 airfoil at a Reynolds number of 20,000 is used for all cases, and a parameter space encompassing a range of values for various kinematic terms is chosen as described in Sect. 4.1.

4.1 Definition of motion kinematics

Combinations of pitch and plunge maneuvers are considered for the parametric study. Both these motions are generated with a modified version of the Eldredge function which produces a ramp motion with smoothed corner [20,31] maneuvers. The pitch histories are given by:

$$\alpha = \alpha_{\text{start}} + \frac{K_\alpha}{a_s}\left[\frac{\cosh(a_s(t^* - t_1^*))}{\cosh(a_s(t^* - t_2^*))}\right] + \frac{\alpha_{\text{amp}}}{2} \tag{12}$$

where a_s is the smoothing parameter from Granlund et al. [29] defined as:

$$a_s = \frac{\pi^2 K_\alpha}{2\alpha_{\text{amp}}(1-\sigma)} \tag{13}$$

and

$$t_2^* = t_1^* + \frac{\alpha_{\text{amp}}}{2K_\alpha} \tag{14}$$

In these equations, t_1^* denotes the time at start of ramp and t_2^* denotes the time at end of ramp. In all simulations in this paper, t_1^* is taken as 5.0 to generate a steady starting solution and hence minimize the effect of starting vortices on the solution. The parameter σ is a nondimensional measure of smoothing and is equal to

Table 1 Base parameter set used to study LEV initiation in low-Reynolds-number flow

Parameter	Symbol	Value
Reynolds number	Re	20,000
Start time of ramp	t_1^*	5.0
Smoothing parameter	σ	0.8
Initial pitch angle	$\alpha_{\text{start}}(^\circ)$	0
Pitch amplitude	$\alpha_{\text{amp}}(^\circ)$	30
Pitch rate	$K_\alpha = \frac{\dot{\alpha}c}{2U}$	0.20
Pivot location	x_p/c	0.25
Plunge amplitude	$(h/c)_{\text{amp}}$	0.0
Plunge rate	$K_h = \frac{\dot{h}}{2U}$	0.0

Table 2 Parameter variations used to study LEV initiation in low-Reynolds-number flow (baseline values are in bold)

Case study number	Variable parameter	Values
1	Pivot location (x_p/c)	0.0, **0.25**, 0.75
2	Pitch rate (K_α)	0.01, 0.03, 0.05, 0.1, **0.2**, 0.4
3	Initial pitch angle (α_{start})	10, 5, **0**, −5, −10, −15
4	Pitch–plunge combination	$\alpha_{\text{amp}} = 30$, $K_\alpha = 0.1$, $(h/c)_{\text{amp}} = -0.1$, $K_h = 0.0191$

0.8 in all kinematics considered here. K_α is the reduced frequency of pitch. The term α_{start} is used to generate kinematics where the ramp starts from a nonzero value.

The plunge kinematics are constructed with the same equations, by replacing α with h/c, K_α with K_h and α_{amp} with $(h/c)_{\text{amp}}$. $(h/c)_{\text{start}}$ is not used (always 0). As the plunge motion is in combination with pitch in this study, the reduced frequency for plunge is chosen such that the pitch and plunge ramps occupy the same nondimensional time ($K_h = K_\alpha * (h/c)_{\text{amp}}/\alpha_{\text{amp}}$). Hence, Eqs. 13 and 14 are not altered. The variation in plunge is given by,

$$\frac{h}{c} = \frac{K_\alpha (h/c)_{\text{amp}}}{a_s \alpha_{\text{amp}}} \left[\frac{\cosh(a_s(t^* - t_1^*))}{\cosh(a_s(t^* - t_2^*))} \right] + \frac{(h/c)_{\text{amp}}}{2} \tag{15}$$

A typical pitch-only ramp motion, starting at $\alpha_{\text{start}} = 0$, with pitch amplitude $\alpha_{\text{amp}} = 30^\circ$, reduced frequency $K_\alpha = 0.2$ and pivoted at quarter chord is considered as a baseline for the parametric study. The detailed definition of this case is given in Table 1.

The parameter space for case studies 1–3 is constructed by considering variations in pitch-axis location, pitch reduced frequency and pitch start angles with respect to the baseline case. In case study 4, a pitch–plunge combination is compared to the baseline case. In keeping with the bounds of the experimental apparatus with respect to plunge maneuvers, the K_α for the pitch–plunge combination was chosen to be 0.1 rather than the baseline value of 0.2. As mentioned previously, the K_h is calculated such that the pitch and plunge ramps occupy the same nondimensional time ($K_h = K_\alpha * (h/c)_{\text{amp}}/\alpha_{\text{amp}}$). The kinematics for the four case studies are listed in Table 2.

For all kinematics, the time instants and corresponding pitch angles at which LEV formation is initiated are determined using experiments and CFD, and the LESP values at these pitch angles are determined from theory. Skin friction coefficient data from CFD are used to quantitatively identify the initiation of LEV formation. Experimental data are used to mutually validate the CFD and qualitatively study the initiation of LEV formation for all kinematics. The identification of LEV initiation using skin friction data are illustrated with the baseline case in Sect. 4.2. The results from the four parametric studies are then presented in Sect. 4.3 with specific emphasis on the pitch angle for LEV initiation with the objective of establishing the envelope of validity of the LESP hypothesis. Section 4.4 presents the results from all four case studies in combination. Finally, Sect. 4.5 discusses two design cases in which plunge motions are added to the baseline pitch motion to alter the occurrence of LEV formation.

4.2 Identification of LEV initiation from CFD data

The procedure used in this research for identifying the initiation of LEV formation from CFD skin friction information is illustrated here with the baseline case listed in Sect. 4.1. Figure 3 shows the LESP and pitch

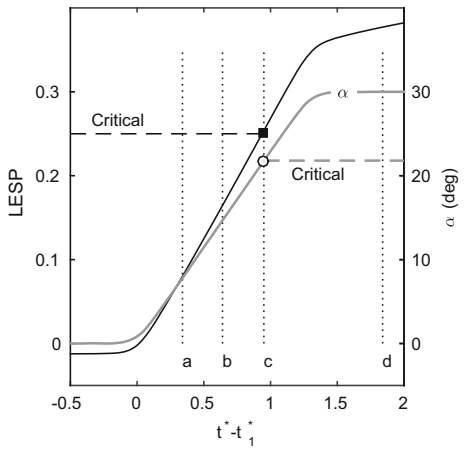

Fig. 3 Pitch angle variation, and LESP history from inviscid theory for the baseline case. The four times instants marked (*a–d*) are used to discuss LEV initiation. The LESP value at instant (*c*) corresponding to LEV initiation from CFD is termed the critical LESP. This critical LESP and the corresponding α are *marked* in the figure

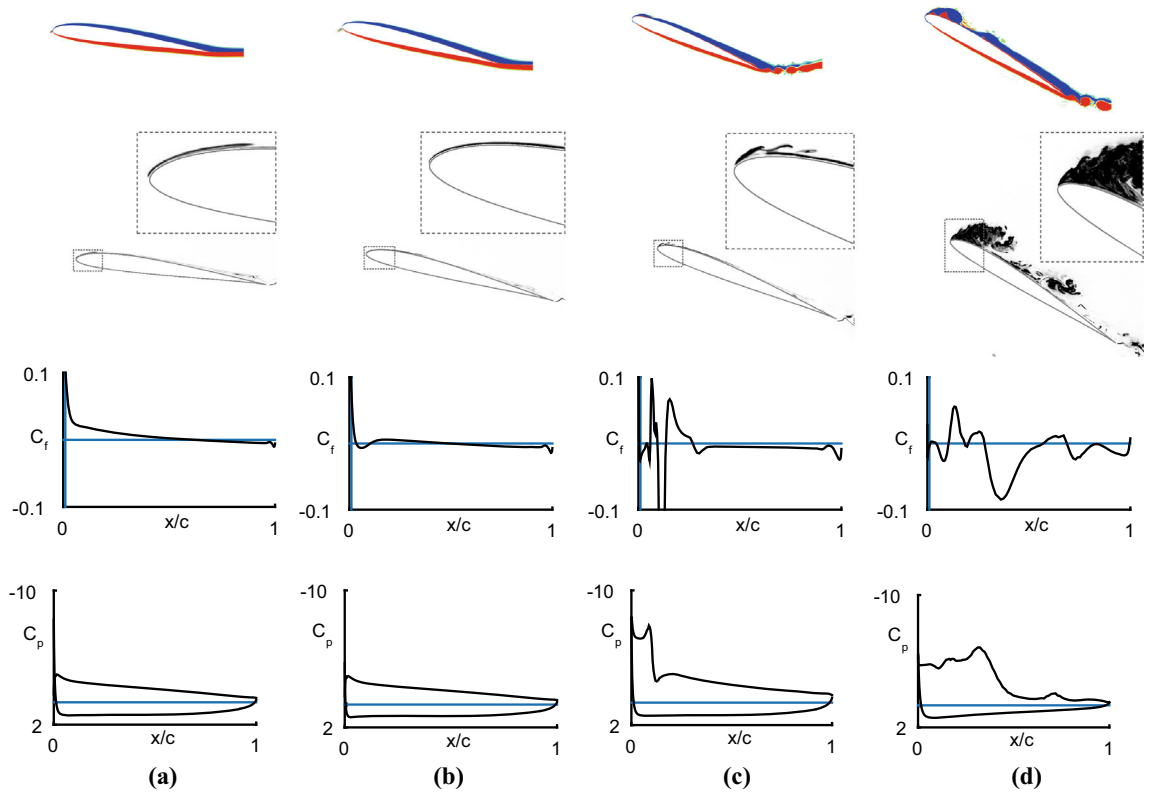

Fig. 4 Baseline case: Vorticity plots from CFD (*first row*), flow visualization from experiment (*second row*), upper surface C_f (*third row*) and *upper* and *lower* surface C_p (*fourth row*) plots from CFD. The four columns (**a–d**) correspond to the time instants marked in Fig. 3. **a** $\alpha = 7.8°$ **b** $\alpha = 14.7°$ **c** $\alpha = 21.7°$ **d** $\alpha = 30.0°$

angle variation against time for this case. In this figure, and in all figures with a time axis in this paper, the x-axis shows $t^* - t_1^*$ so that the ramps begin at 0 on this axis. We emphasize that, in this figure and all the other LESP variations in this paper, the LESP is calculated using the inviscid unsteady thin-airfoil theory. Unlike in the LDVM low-order method [56], there is no discrete vortex shedding to model the LEV shedding. The current LESP prediction is, therefore, valid only until the onset of LEV shedding even though the LESP variations are plotted for the entire motion. For the current purposes of studying the factors leading to initiation

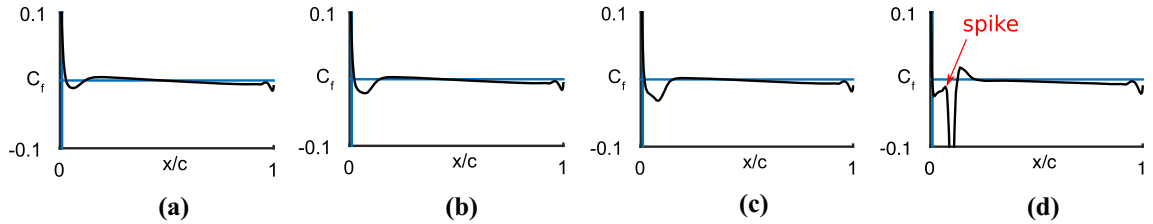

Fig. 5 Baseline case: Skin friction coefficients at four intermediary points between the onset of reversed flow and the initiation of LEV formation, i.e., between time instants (**b**) and (**c**) in Fig. 4. **a** $\alpha = 16.0°$ **b** $\alpha = 17.4°$ **c** $\alpha = 18.8°$ **d** $\alpha = 20.2°$

of LEV formation, however, this inviscid LESP is the appropriate. Four time instants (a)–(d) are marked on this plot to help describe the process used in quantitatively identifying LEV initiation from CFD data.

Figure 4 presents results from experiments and CFD for the baseline case at four instants during the motion. The upper surface skin friction (C_f) distributions from CFD (on the third row of the figure) are examined at various time instants of the motion to identify several key steps that lead to the formation of the LEV. The flow features leading to LEV formation have been discussed by several authors [2,17,27,71]. The four time instants at (a)–(d), also marked in Fig. 3, are used to highlight the following flow features:

(a) *Attached flow* Before the initiation of the LEV formation, the flow is attached at the leading edge. The attached boundary layer is thin and the C_f is positive.
(b) *Onset of reversed flow* LEV formation is first preceded by the formation of a small region of reversed flow near the leading edge of the airfoil, signaled by appearance of counterclockwise vorticity near the surface and a small region of negative C_f.
(c) *Initiation of LEV formation* Next, a small region of clockwise vorticity starts to develop at the surface within the region of counterclockwise vorticity seen in (b). This manifests as a spike in the negative C_f distribution that reaches up to zero and subsequently becomes a region of positive C_f within the region of negative C_f distribution. This flow feature signals the formation of the shear layer in which there is an eruption of surface flow into the mainstream. As in previous work [58,60], the instant when the spike in the negative C_f region first reaches the zero value is taken as the time corresponding to initiation of LEV formation. In Fig. 5, the C_f distributions are presented at four intermediate points between time instants (b) and (c). These show the process where a spike develops within the region of negative C_f, reaching up to zero and subsequently crossing it at instant (c). This C_f condition is used as a quantitative way to consistently identify the time instant of LEV initiation. We note that the eruption of vorticity from the leading edge is visible in the vorticity (CFD) and flow visualization (experiment) plots at this instant.
(d) *Formation and feeding of the LEV* The eruption of surface flow, initiated in (c), results in a plume of clockwise vorticity flowing into the mainstream. During these time instants, there are several spikes in the C_f distribution corresponding to positive-C_f regions embedded within a larger negative-C_f region.

In the following parametric studies, we refer to the LEV initiation condition of the baseline case as the critical condition against which we assess LEV initiation for all other cases. The LESP at the instant of LEV initiation for the baseline case is hence the critical LESP value (=0.25) as illustrated in Fig. 3.

4.3 Parametric studies of LEV initiation

4.3.1 Case study 1: Effect of pivot location

In this study, the effect of pitch-axis location on LEV initiation in unsteady maneuvers is examined. In addition to the baseline case (quarter chord pivot), two cases with modified pivot locations (leading-edge and three-quarter-chord) are considered. The pitch angle during the ramp maneuver at which LEV formation is initiated (as determined using the procedure described in Sect. 4.2) is plotted for all three cases in Fig. 6. As the pivot location is varied along the chord from leading to trailing edge, the pitch angle at LEV initiation is seen to increase. This behavior is due to the effect of increased motion-induced "downwash" at the leading edge as the pivot is moved aftward, a trend known from earlier works [46,57]. Clearly, there is no obvious relation between initiation of LEV formation and the values of the pitch angle at that time instant. In Fig. 7, the time variation of LESP for the three kinematics from unsteady thin-airfoil theory are co-plotted with the instants of

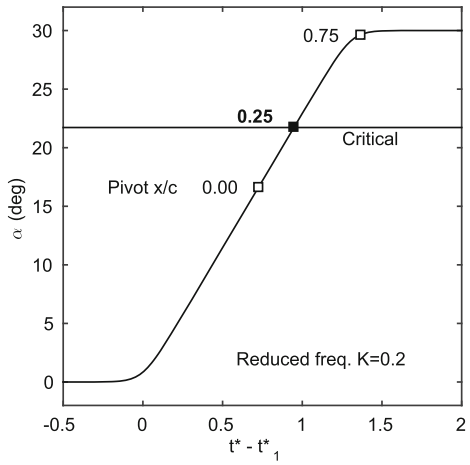

Fig. 6 Case study 1, effect of pivot location: pitch angle variation with time and pitch angles corresponding to LEV initiation. Baseline value is *bold*

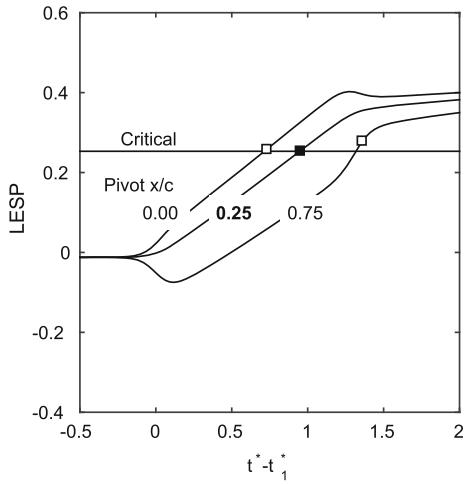

Fig. 7 Case study 1, effect of pivot location: LESP variation with time and LESP values corresponding to LEV initiation. Baseline value is *bold*

LEV formation marked. It is seen that the initiation of upper surface LEV formation occurs at a near-constant LESP value.

More insight into the LEV formation and shedding process is gained by analyzing the experimental and numerical results together. Flow visualization plots from experiment, vorticity plots from CFD, pressure coefficient (upper and lower surfaces) and skin friction coefficient (upper surface) distributions from CFD at the instants of LEV initiation for the three cases are shown in Fig. 8. At the time of LEV initiation, we see that the C_p and C_f distributions for the three cases are qualitatively similar. The vorticity and flow visualization plots show that the flow is attached over most of the airfoil for all three cases, as is expected for the high-reduced-frequency case ($K = 0.2$). This explains the LESP hypothesis holding valid in this case study, as the theory is derived on the basis of an attached flow assumption.

The same plots from CFD and experiment, at some time after the initiation of LEV formation, are shown in Fig. 9. The time instant is chosen as that when the inviscid LESP value is greater than $\mathrm{LESP}_\mathrm{crit}$ by a value of 0.05. The LESP is a measure of the velocity at the leading edge and also the velocity at the start of the shear layer emanating from the leading edge. Now, the flux of vorticity into the free shear layer (LEV) may be related to the shear-layer edge velocity by the relation derived by Sears [63] which was also experimentally observed by Fage and Johansen [24],

$$\frac{\mathrm{d}\Gamma_\mathrm{sh}}{\mathrm{d}t} = \frac{1}{2}U_\mathrm{sh}^2 \tag{16}$$

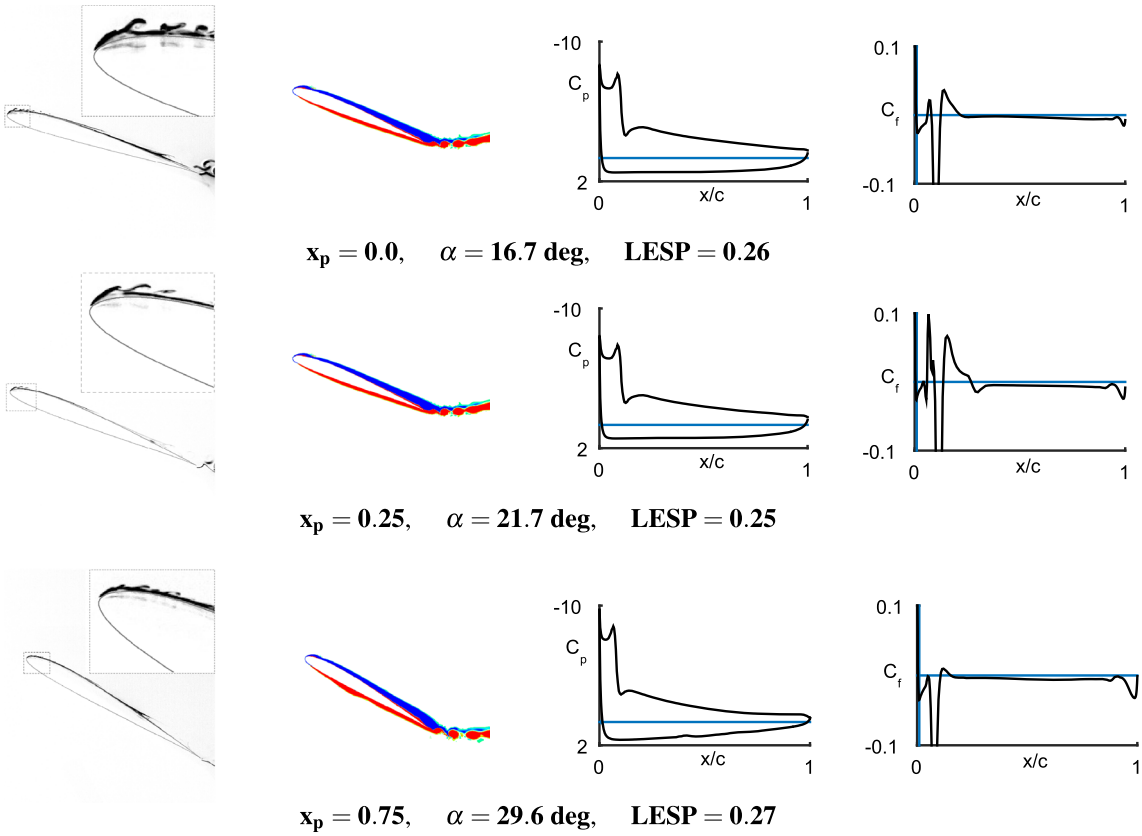

Fig. 8 Case study 1, effect of pivot location, at the instants of LEV initiation: *left* to *right*—flow visualization from experiment, vorticity plots from CFD, C_p (*upper* and *lower* surfaces) and C_f (*upper* surface) distributions from CFD

This relation has also been used to model vortex shedding from edges in discrete vortex methods such as those by Sarpkaya [62] and Katz [37]. The instants when the LESP is greater than $\text{LESP}_{\text{crit}}$ by a certain constant value thus should correspond to times when approximately equal vorticity has been shed into the LEVs in all cases. Strictly, the LESP curves in Fig. 7 are only valid until the instant of LEV initiation, as LEV shedding which occurs after this instant is not modeled. Still, $\Delta\text{LESP} = 0.05$ is chosen as an approximate measure of when all cases would be at the same stage of vortex development, irrespective of motion parameters. Figure 9 shows that the LEV structures and C_p distributions are similar for the three cases with different pitch-axis locations. Further, all three cases show the presence of a concentrated LEV with no noticeable flow separation over the rest of the airfoil.

We note here that the results from this case study confirm the well-known result that the pitch angle at LEV initiation increases as the pitch axis is moved aft on the airfoil (seen in Fig. 6). This result can be elegantly derived using the LESP theory. Using Eqs. 4 and 5, and assuming a flat plate, small angle deflections, no plunge and no wake influence,

$$\text{LESP} = A_0 = \alpha + 2K_\alpha \left(\frac{1}{2} - \frac{x_p}{c}\right) \tag{17}$$

Using the hypothesis that the LESP at LEV initiation is equal to $\text{LESP}_{\text{crit}}$ for all cases with the same airfoil and Reynolds number, the angles of attack at LEV initiation for various pitch axes (with the same pitch rate) may be related as,

$$\text{LESP}_{\text{crit}} = \alpha_{\text{crit}_1} + 2K_\alpha \left(\frac{1}{2} - \frac{x_{p_1}}{c}\right) = \alpha_{\text{crit}_2} + 2K_\alpha \left(\frac{1}{2} - \frac{x_{p_2}}{c}\right) \tag{18}$$

Substituting for values of pitch-axis locations yields the result that the pitch angle at LEV initiation increases as pitch axis is moved aft. The LESP can essentially be regarded as a more general effective angle of attack which also accounts for wake-induced velocities and which holds true even without the assumptions of flat

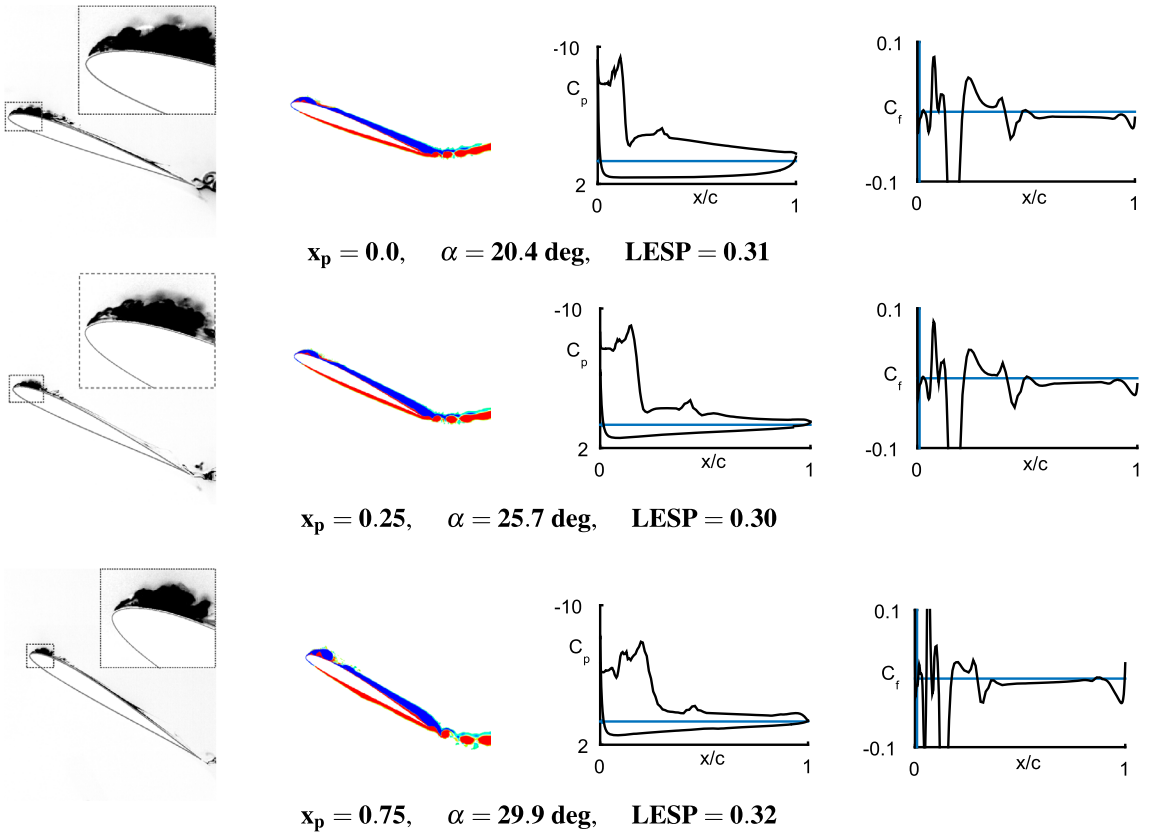

Fig. 9 Case study 1, effect of pivot location, at $\Delta\text{LESP} = 0.05$ after the instants of LEV initiation: *left* to *right*—flow visualization from experiment, vorticity plots from CFD, C_p (*upper* and *lower* surfaces) and C_f (*upper* surface) distributions from CFD

plate, small angle deflections, no plunge, and no wake influence. Similar relations between pitch angles at LEV initiation can be derived for varying pitch rates and other parameters.

4.3.2 Case study 2: Effect of pitch rate

In this case study, the effect of pitch rate on LEV formation in unsteady maneuvers is investigated. In addition to the baseline case ($K = 0.2$), five cases with modified pitch rates ($K = 0.01$, 0.03, 0.05, 0.1 and 0.4) are considered.

The pitch angles during the ramp motion at which LEV formation is initiated (as determined using the procedure described in Sect. 4.2) for the six cases are plotted in Fig. 10. The pitch angle at LEV initiation is seen to increase with increasing pitch rate. High-pitch rates hence serve to keep the flow attached to the airfoil, which is well known from dynamic stall research (e.g., Ref. [39]). In Fig. 11, the time variation of LESP for the six kinematics from unsteady thin-airfoil theory is co-plotted with the instants of LEV formation marked. In this case, we do not observe a near-constant critical LESP value, but a trend where critical LESP increases with increasing pitch rate. This result is analyzed in detail by studying flow features from experiments and CFD in the remainder of this section.

Flow visualization plots from experiment, vorticity plots from CFD, pressure-coefficient (upper and lower surfaces) and skin friction coefficient (upper surface) distributions from CFD at the instants of LEV initiation for the six cases are shown in Fig. 12. The first three cases with pitch rates of 0.01, 0.03 and 0.05, respectively, are seen to exhibit significant boundary-layer thickening and flow separation on the aft half of the upper surface of the airfoil surface at the time of LEV initiation. We do not expect the LESP hypothesis to hold true for these cases, as the underlying unsteady thin-airfoil theory assumes attached flow over the whole airfoil and is hence not valid. If trailing-edge separation were modeled in the calculation of LESP, the hypothesis may hold true even for the slow pitch rate cases, although this needs to be confirmed with further study. The C_p distributions for the six cases show a clear trend, with higher pitch rates resulting in a greater values of suction at the leading

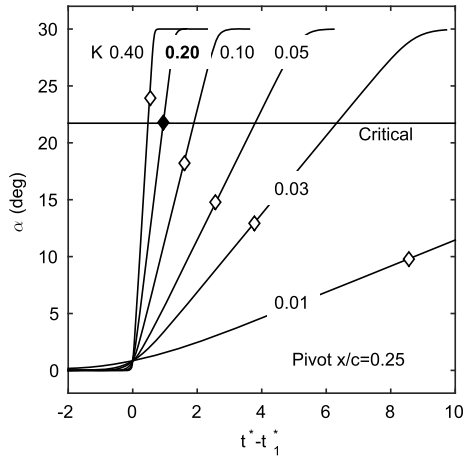

Fig. 10 Case study 2, effect of pitch rate: pitch angle variation with time and pitch angles corresponding to LEV initiation. Baseline value is *bold*

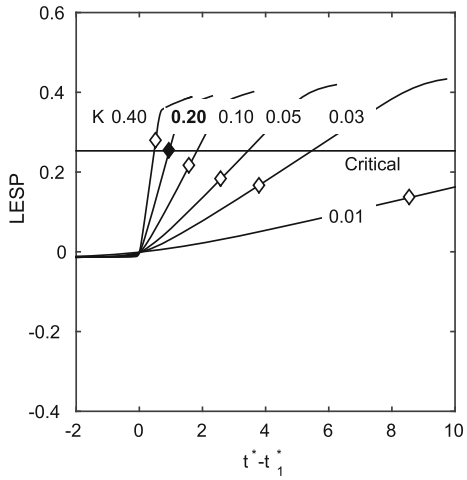

Fig. 11 Case study 2, effect of pitch rate: LESP variation with time and LESP values corresponding to LEV initiation. Baseline value is *bold*

edge of the airfoil. The C_f distributions and the C_f-spike which is used to identify LEV initiation also show clear trends with the spike moving aft on the airfoil and getting broader/diffused with decreasing pitch rate. The reduced level of trailing-edge flow separation with increasing pitch rate has been well documented in dynamic stall studies, and can also be observed in Fig. 12. As trailing-edge separation is not modeled in the current method, this helps explain the absence of a near-constant critical LESP for kinematics with varying pitch rates. Nevertheless, as will be demonstrated in Sect. 4.4, this concept may still be employed with reasonable level of accuracy for high-pitch-rate kinematics.

The same plots from CFD and experiment, at some time after the initiation of LEV formation, are shown in Fig. 13. The time instant, as done in case study 1, is chosen as that when the inviscid LESP value is greater than $\text{LESP}_{\text{crit}}$ by a value of 0.05. The LEV structures for the six cases exhibit a trend of being more concentrated with increasing pitch rate. For the first case with $K = 0.01$, the pitch rate is so slow that the airfoil is "nearly steady" and displays a bluff-body-type flow. The second and third cases show distinct LEVs, along with the presence of flow separation over the rest of the airfoil. The final three cases each have a concentrated LEV with no significant separation over the rest of the airfoil surface. For these cases, it is shown in Sect. 4.4 that the LESP may still be used to predict LEV initiation.

4.3.3 Case study 3: Effect of initial pitch angle

In case study 3, the influence of boundary-layer development and flow separation on LEV initiation is investigated by starting the pitch ramps from nonzero values. In addition to the baseline case (which starts from a

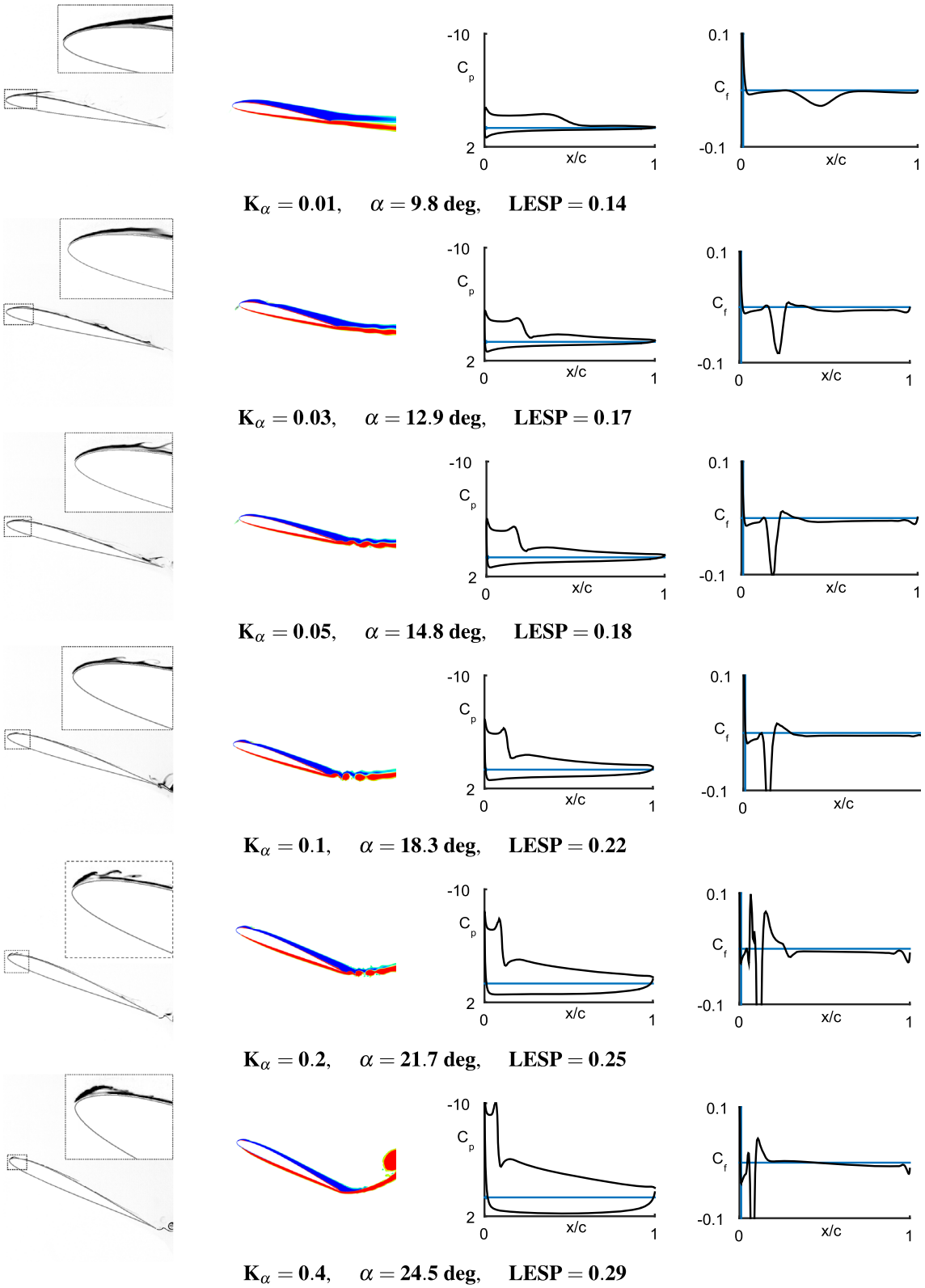

Fig. 12 Case study 2, effect of pitch rate, at the instants of LEV initiation: *left* to *right*—flow visualization from experiment, vorticity plots from CFD, C_p (*upper* and *lower* surfaces) and C_f (*upper* surface) distributions from CFD

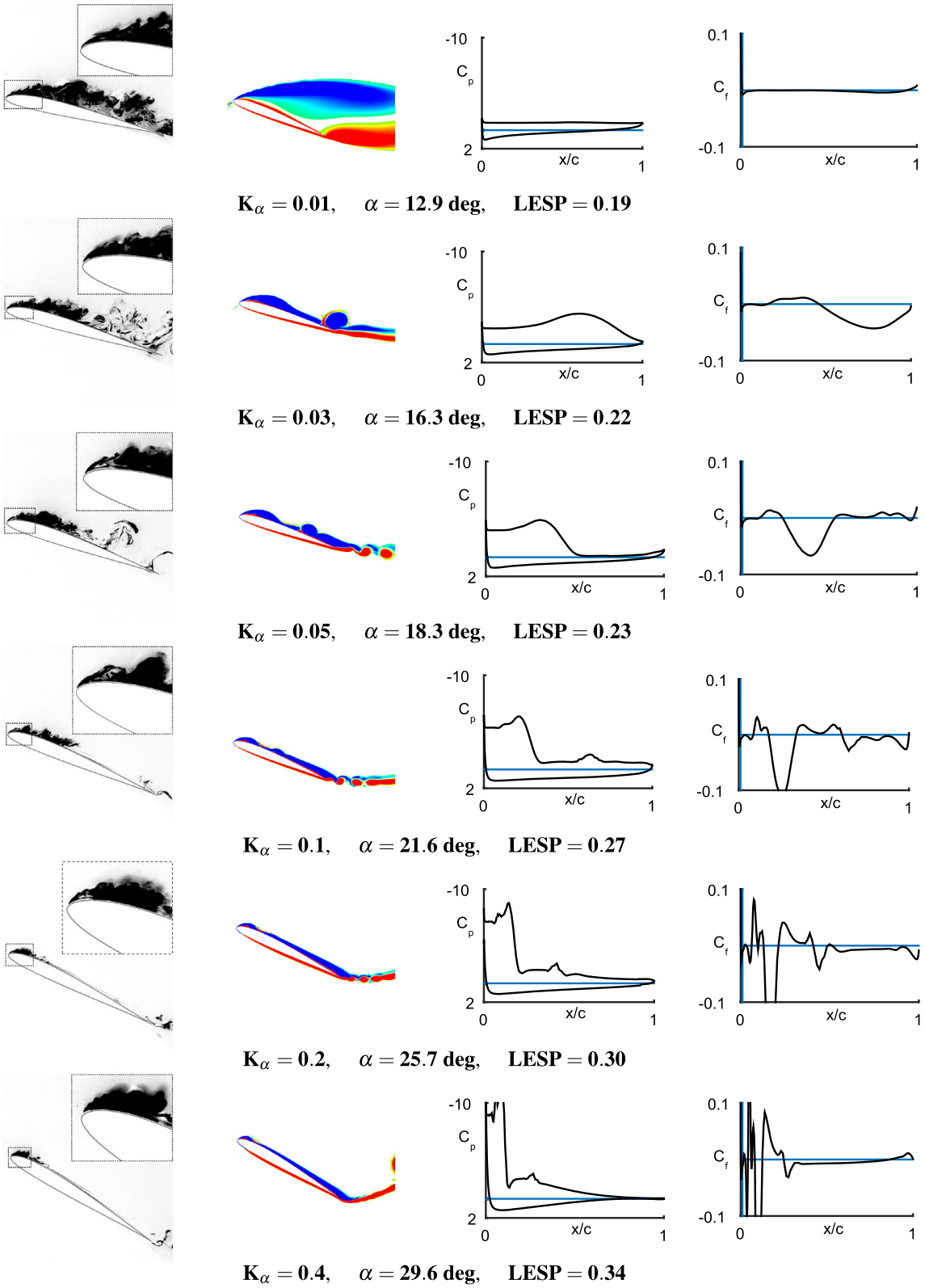

$\mathbf{K_\alpha = 0.01}$, $\mathbf{\alpha = 12.9\ deg}$, $\mathbf{LESP = 0.19}$

$\mathbf{K_\alpha = 0.03}$, $\mathbf{\alpha = 16.3\ deg}$, $\mathbf{LESP = 0.22}$

$\mathbf{K_\alpha = 0.05}$, $\mathbf{\alpha = 18.3\ deg}$, $\mathbf{LESP = 0.23}$

$\mathbf{K_\alpha = 0.1}$, $\mathbf{\alpha = 21.6\ deg}$, $\mathbf{LESP = 0.27}$

$\mathbf{K_\alpha = 0.2}$, $\mathbf{\alpha = 25.7\ deg}$, $\mathbf{LESP = 0.30}$

$\mathbf{K_\alpha = 0.4}$, $\mathbf{\alpha = 29.6\ deg}$, $\mathbf{LESP = 0.34}$

Fig. 13 Case study 2, effect of pitch rate, at ΔLESP = 0.05 after the instants of LEV initiation: *left* to *right*—flow visualization from experiment, vorticity plots from CFD, C_p (*upper* and *lower* surfaces) and C_f (*upper* surface) distributions from CFD

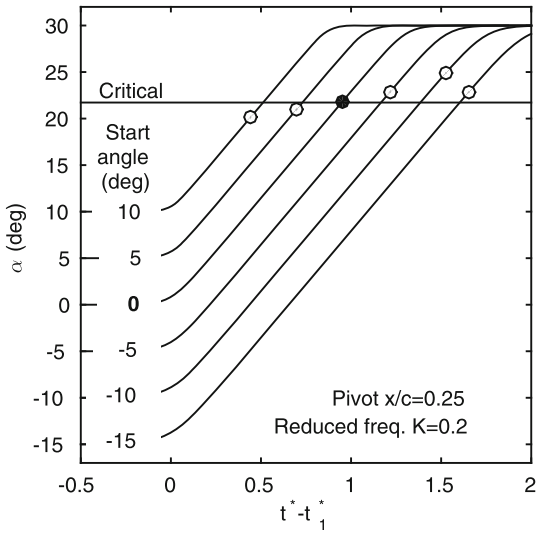

Fig. 14 Case study 3, effect of initial pitch angle: pitch angle variation with time and pitch angles corresponding to LEV initiation. Baseline value is *bold*

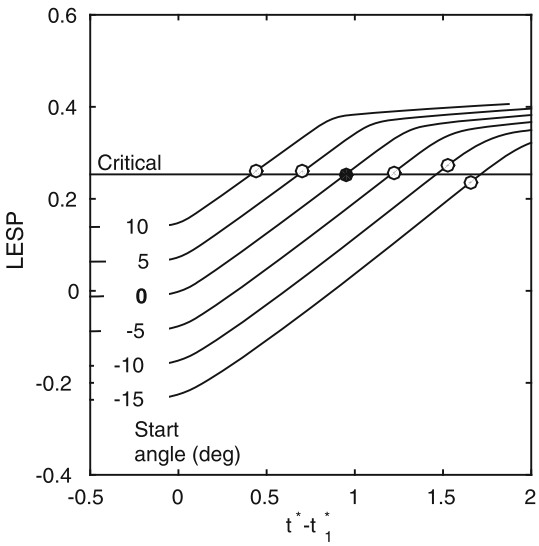

Fig. 15 Case study 3, effect of initial pitch angle: LESP variation with time and LESP values corresponding to LEV initiation. Baseline value is *bold*

pitch angle of 0), five cases starting with starting pitch angles of 10°, 5°, −5°, −10° and −15° are used. We note that 10° is close to the static stall angle of the SD7003 airfoil (≈11° [64]). The pitch angle histories for these cases and the angles at which LEV formation is initiated are plotted for all six cases in Fig. 14.

In all cases, a steady boundary layer is established at the starting pitch angle before the ramp is initiated. The results show some variation in the pitch angles at which LEV formation is initiated for these cases. There is an apparent trend of delayed LEV initiation for all but the $\alpha_{\text{start}} = -15$ case, which starts with large pressure-side separation. Figure 15 displays the time variation of LESP as determined from theory for the six cases. For cases starting with nonzero pitch angles, the LESP values are seen to be close to the baseline value.

Flow visualization plots from experiment, vorticity plots from CFD, C_{p} (upper and lower surfaces) and C_{f} (upper surface) distributions from CFD at the instants of LEV initiation for cases study 3 are shown in Fig. 16. For the cases with start angles of −5°, −10°, and −15°, flow visualization images for both upper and lower surfaces are shown because these cases have significant lower surface separation. The first two cases (starting at 10° and 5°) exhibit flow separation on the airfoil upper surface at the time of LEV initiation, while the final three cases (starting at −5°, −10° and −15°) exhibit separated flow on the lower surface.

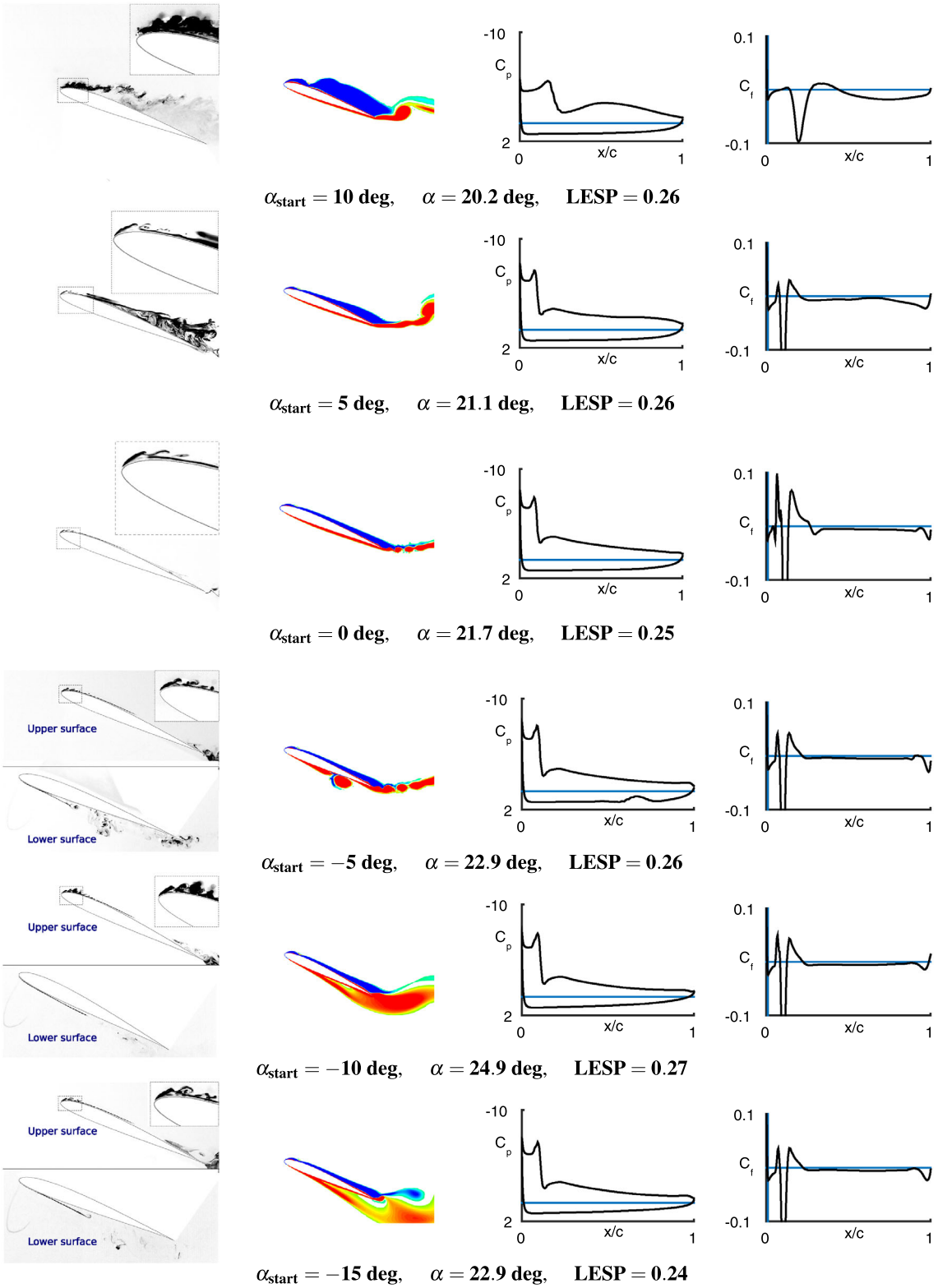

Fig. 16 Case study 3, effect of initial pitch angle, at the instants of LEV initiation: *left* to *right*—flow visualization from experiment, vorticity plots from CFD, C_p (*upper* and *lower* surfaces) and C_f (*upper* surface) distributions from CFD

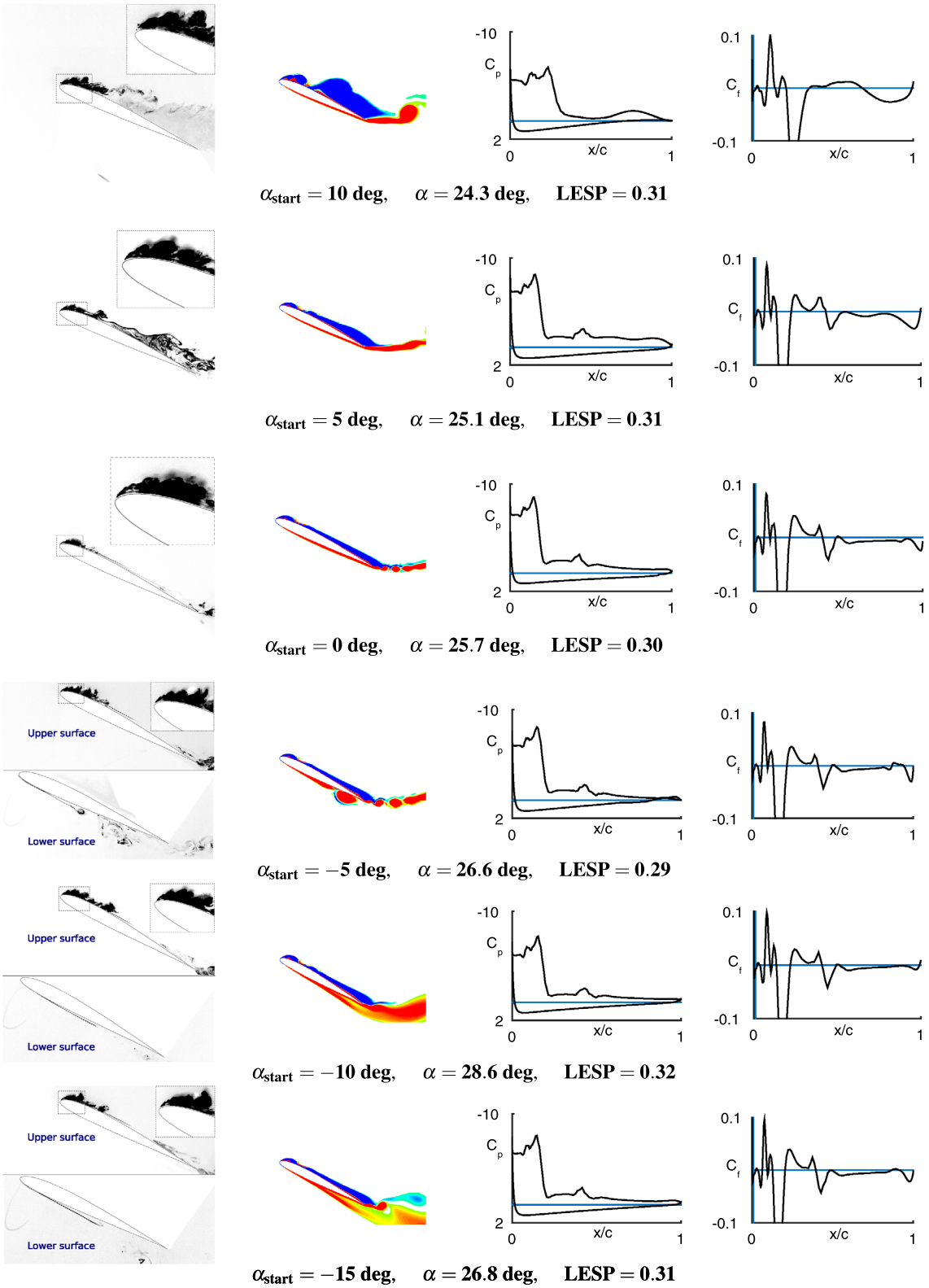

Fig. 17 Case study 3, effect of initial pitch angle, at ΔLESP $= 0.05$ after the instants of LEV initiation: *left* to *right*—flow visualization from experiment, vorticity plots from CFD, C_p (*upper* and *lower* surfaces) and C_f (*upper* surface) distributions from CFD

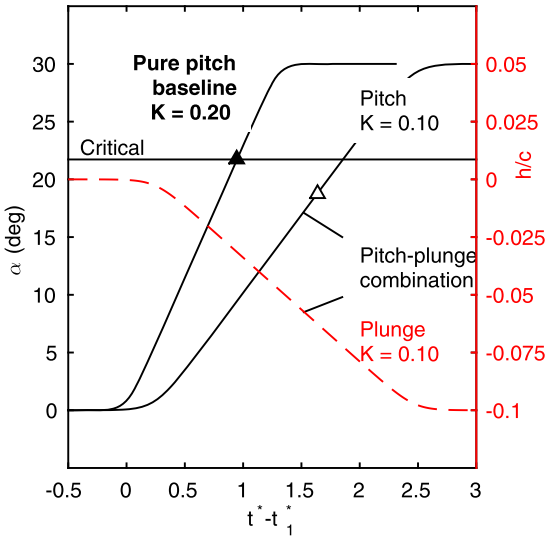

Fig. 18 Case study 4, baseline versus pitch–plunge combination: pitch angle/plunge amplitude variation with time and pitch angles corresponding to LEV initiation. Baseline value is *bold*

The same plots from CFD and experiment, at an instant after the initiation of LEV formation when the inviscid LESP value is greater than $\text{LESP}_{\text{crit}}$ by a value of 0.05, are shown in Fig. 17. All the cases exhibit a concentrated vortex, with the first two also showing significant trailing-edge separation. The LESP hypothesis is however seen to hold for all cases (Fig. 15) in contrast to the slow ramp cases in Sect. 4.3.2 which also had significant trailing-edge separation. Hence, the presence of separated shear layers/thick boundary layers as an initial condition does not appear to affect LEV initiation as much as the effect that the dynamic flow separation on the airfoil surface had at low pitch rates.

4.3.4 Case study 4: Pitch–plunge combination

In this study, we aim to assess whether the LESP hypothesis (LEV initiation occurring at the same critical value of LESP) applies not only to various pitching maneuvers, but also to any arbitrary unsteady maneuver. In addition to the baseline case, a pitch–plunge combination is considered. The latter has a pitch amplitude of 30°, plunge amplitude/chord of −0.1, and reduced frequency (in pitch) of 0.1 as given in Table 2. The pitch angle histories for the two cases and the angles at which LEV formation is initiated are plotted in Fig. 18.

Figure 19 displays the time variation of LESP as determined from theory for the two cases, and the LESP values at the instant of LEV initiation as determined from CFD (Sect. 4.2). LEV initiation in both cases is seen to occur at the same LESP value.

As done in the earlier case studies, flow visualization from experiment, vorticity plots from CFD, C_{p}, and C_{f} distributions from CFD at the instants of LEV initiation for the two cases are shown in Fig. 20. Despite LEV initiation occurring at different angles of attack, the C_{f} distributions for the two cases are similar at the instant of LEV initiation, which also corresponds to the same critical value of LESP as seen in Fig. 19.

The same plots from CFD and experiment for the two cases, at a time after initiation of LEV formation when the inviscid LESP value is greater than $\text{LESP}_{\text{crit}}$ by a value of 0.05, are shown in Fig. 21. The vortex development for the two cases is seen to be quite different owing to the different types of motion and the different reduced frequencies. While the baseline case exhibits a small concentrated vortex, the pitch–plunge combination evinces a more diffused LEV accompanied by trailing-edge flow separation.

4.4 Assessment of the LESP hypothesis

The results from all the parametric studies are compiled here with the aim of assessing the LESP hypothesis. Two approaches are used to assess the effectiveness of the hypothesis. In the first approach, the theoretical predictions of pitch angles corresponding to LEV formation for all motions are compared against the corresponding CFD predictions. For the theoretical predictions, a single value of $\text{LESP}_{\text{crit}}$ corresponding to LEV formation for

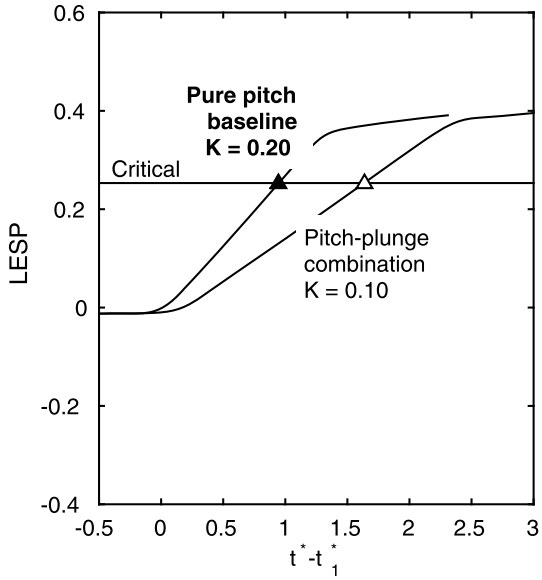

Fig. 19 Case study 4, baseline versus pitch–plunge combination: LESP variation with time and LESP values corresponding to LEV initiation. Baseline value is *bold*

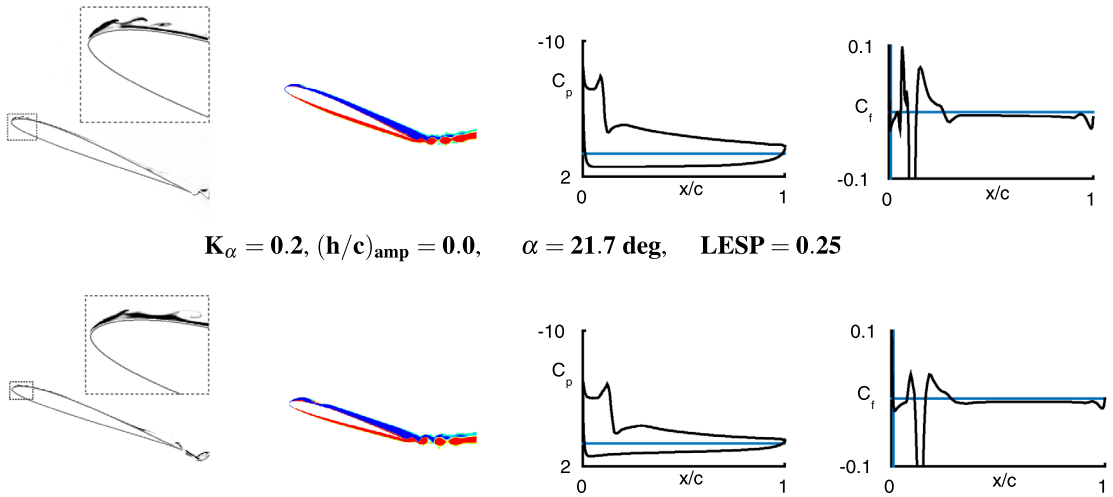

Fig. 20 Case study 4, baseline versus pitch–plunge combination, at the instants of LEV initiation: *left* to *right*—flow visualization from experiment, vorticity plots from CFD, C_p (*upper* and *lower* surfaces) and C_f (*upper* surface) distributions from CFD

the baseline case is used as the critical value for all motions. For any motion, the pitch angle at which the instantaneous LESP equals this baseline $\text{LESP}_{\text{crit}}$ is taken as the theoretical prediction for initiation of LEV formation for that motion. On the other hand, the CFD prediction for this pitch angle is determined using the procedure described in Sect. 4.2. In the second approach, the LESP values corresponding to CFD-predicted time instants of LEV formation for the motions are plotted against the four parameters used in the parametric study.

Figure 22 shows the results of the first approach, with the theoretical predictions on the vertical axis plotted against the CFD predictions on the horizontal axis. Lines indicating deviations of $\pm 1^\circ$ and $\pm 2.5^\circ$ from a perfect correlation are included for comparison. It is seen that, with the exceptions of the three slow-pitch-rate cases from case study 2 ($K = 0.01$, 0.03 and 0.05), the predictions from CFD and theory are within an error margin of $\pm 1^\circ$ for most cases, and within $\pm 2.5^\circ$ for all cases. As discussed in case study 2, the three slow-pitch-rate cases are the ones in which there is significant trailing-edge separation preceding LEV formation. This assessment shows that, so long as LEV formation is not preceded by significant trailing-edge separation, theoretical

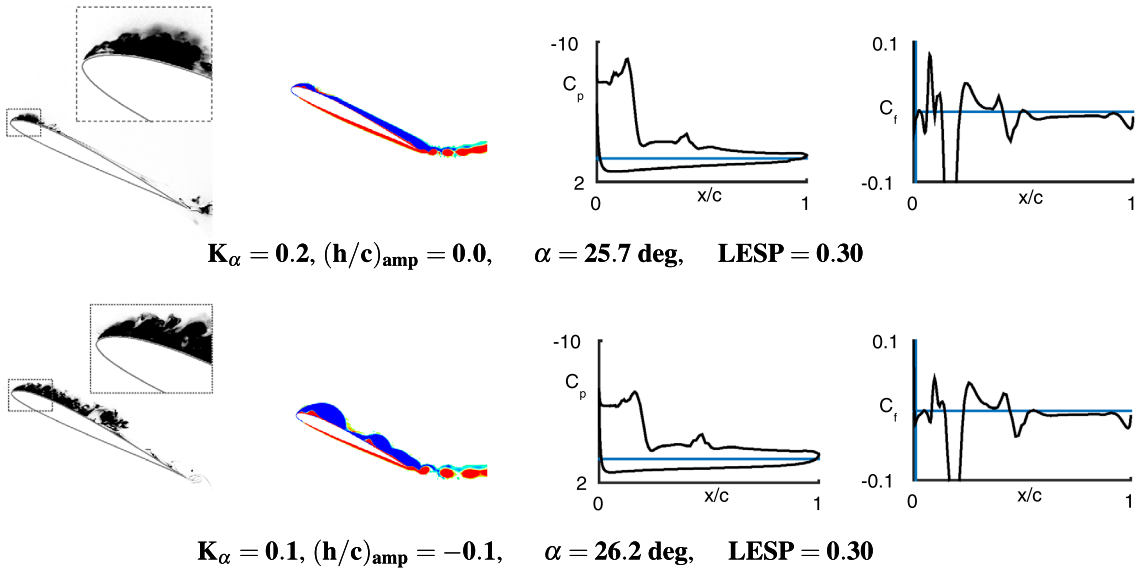

Fig. 21 Case study 4, baseline versus pitch–plunge combination, at ΔLESP = 0.05 after the instants of LEV initiation: *left* to *right*—flow visualization from experiment, vorticity plots from CFD, C_p (*upper* and *lower* surfaces) and C_f (*upper* surface) distributions from CFD

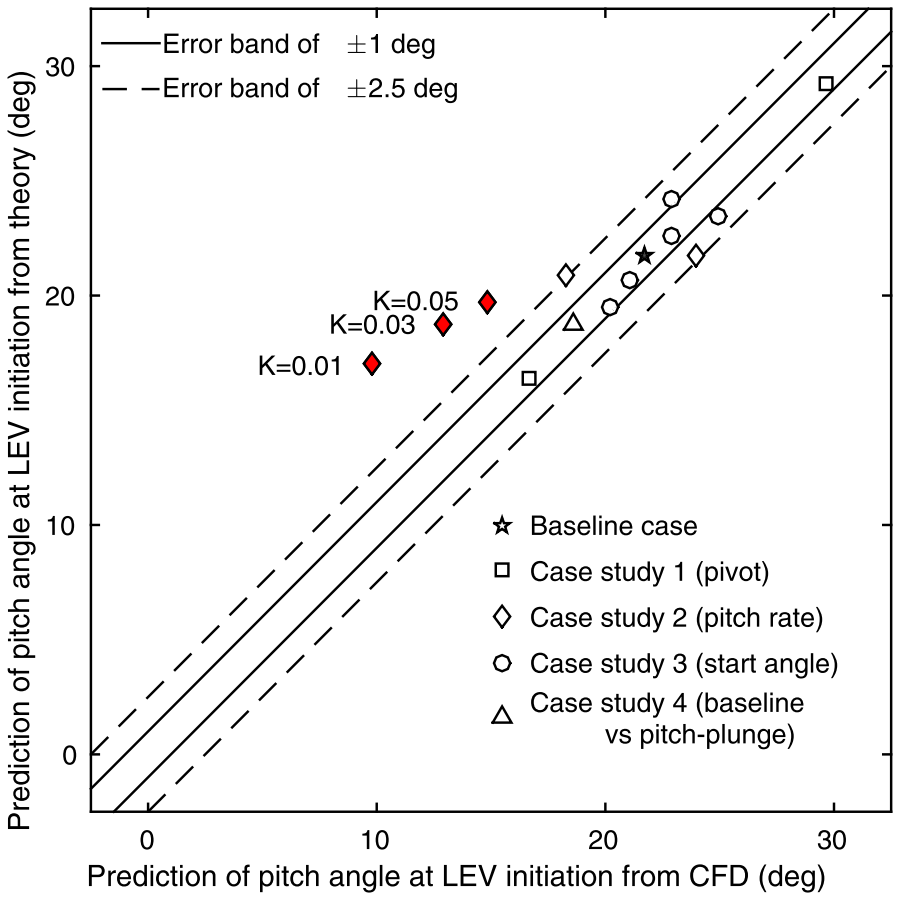

Fig. 22 Pitch angle at the instant of LEV initiation : *x*-axis shows predictions from CFD and *y*-axis shows prediction from theory using $\text{LESP}_{\text{crit}} = 0.25$. The *three red symbols* indicate outliers (color figure online)

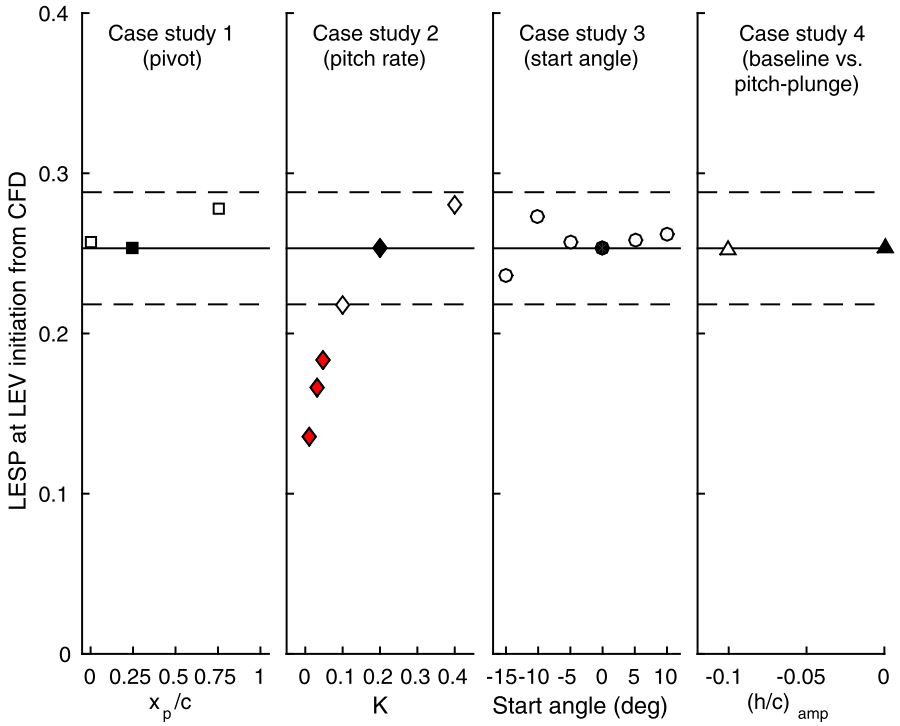

Fig. 23 LESP values at the instant of LEV initiation (as determined from CFD), compiled for all cases considered. Baseline value is *bold*. The *three red symbols* indicate outliers (color figure online)

prediction of LEV formation using a single representative value of $\text{LESP}_{\text{crit}}$ agrees well with CFD predictions for a wide range of motion parameters, verifying the LESP hypothesis.

Figure 23 shows the variations of LESP values at the CFD-predicted time instants of LEV initiation for all the cases with the four parameters: pivot location, pitch rate, start angle, and plunge amplitude. Also shown are the $\text{LESP}_{\text{crit}}$ value of 0.25 for the baseline case and the band of values that correspond to the $\pm 2.5^\circ$ error margin in Fig. 22. It is seen that the LESP variations for case studies 1, 3, and 4 do not have clear patterns and the LESP values for LEV initiation are all close to that for the baseline case and within the error band. For case study 2, we see that the LESP value for LEV initiation increases with increasing pitch rate. One possible reason for this behavior is the progressive decrease in the trailing-edge separation with increasing pitch rate at the time instant of LEV initiation. On the whole, it is seen that with the exception of the three outliers, the LESP values at LEV initiation for all cases lie within 14% of the critical value for the baseline case. In the next section, the use of LESP as a low-order tool for manipulating LEV formation is demonstrated.

4.5 Design of motion kinematics to trigger/suppress LEV formation

In the preceding sections, we showed that the initiation of LEV formation at the leading edge is related to the LESP exceeding a certain critical value. The critical LESP value is a function of the airfoil shape and Reynolds number of operation. Once pre-determined using experimental or computational methods, the critical LESP value corresponds to onset of LEV formation, irrespective of motion kinematics. Hence LEV occurrence may be controlled by suitably altering the motion kinematics such that the LESP critical value is attained at a desired time instant.

Consider the baseline case in Sect. 4.2, analyzed with CFD—a pitch motion with amplitude of 30°, reduced frequency of 0.2, and pivot about the quarter chord. For these motion kinematics, LEV formation was seen to be initiated on the upper surface at $t^* - t_1^* = 0.95$, $\alpha = 22^\circ$. In this section, we modify the occurrence of LESP variation by superimposing a plunge motion on the baseline case, such that LEV initiation is either advanced or delayed as desired.

As it is well known that (negative) rate of plunge is equivalent to variation in pitch angle [46], the plunge rate is taken to be in the form of an Eldredge-ramp function (same as pitch angle).

$$\frac{\dot{h}}{c} = \frac{K_\alpha (\dot{h}/c)_{\text{amp}}}{a_s \alpha_{\text{amp}}} \left[\frac{\cosh(a_s(t^* - t_1^*))}{\cosh(a_s(t^* - t_2^*))} \right] + \frac{(\dot{h}/c)_{\text{amp}}}{2} \tag{19}$$

The plunge motion to be superimposed on pitch is obtained by integrating the Eldredge-form plunge rate,

$$\frac{h}{c} = \int_0^t \frac{\dot{h}}{c} \mathrm{d}t \tag{20}$$

A Newton iteration is used to determine the value of $(\dot{h}/c)$ such that criteria on LESP are satisfied, using which the plunge motion is then constructed with Eqs. 19 and 20. Recalling that LEV initiation in the baseline case occurs at $t^* - t_1^* = 0.95$, plunge-combined kinematics are constructed such that LEV initiation is shifted to (i) $t^* - t_1^* = 0.5$, and (ii) $t^* - t_1^* = 1.5$. The values of $(\dot{h}/c)$ as determined from the Newton iteration for these two cases (hereafter called "design cases") are -0.5098 and 0.1933 respectively. As expected, the LESP theory predicts a negative plunge (equivalent to positive pitch angle) to advance LEV formation and a

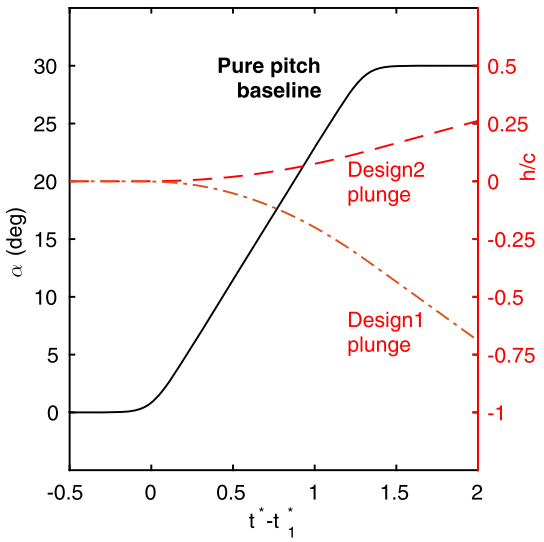

Fig. 24 Pitch amplitude variation with time for the baseline case, and plunge amplitude variations which are used in combination with baseline pitch to generate the two design cases

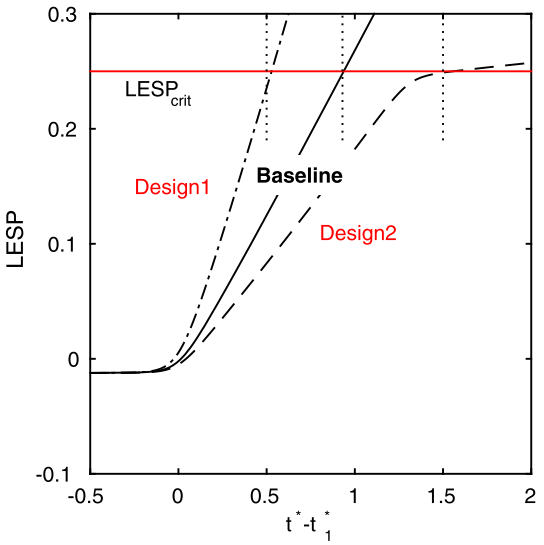

Fig. 25 LESP variation with time for the baseline case and the two design cases. As required by the design criteria, the intersection of instantaneous LESP with critical LESP is at $t^* - t_1^* = 0.5$ and 1.5 respectively

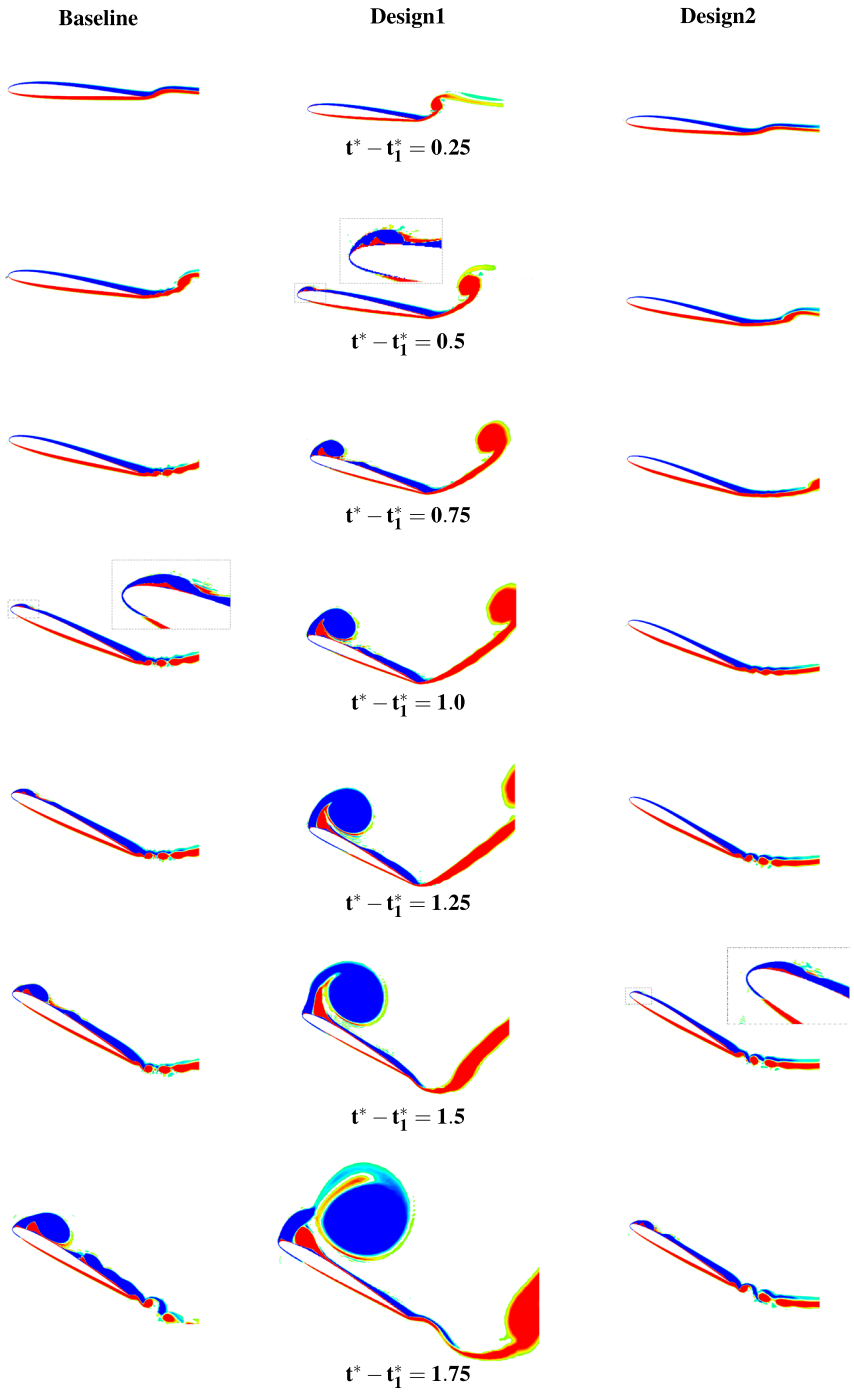

Fig. 26 Vorticity plots from CFD at various instants during the baseline, design1 and design2 cases

positive plunge to delay LEV formation. Figure 24 shows the baseline case (pure pitch), and the two design cases which are constructed by combining the baseline pitch with the two plunge motions shown. Figure 25 illustrates the LESP histories for the baseline motion and two design motions. As required, the LESP values for the design cases cross the critical value at $t^* - t_1^* = 0.5$ and $t^* - t_1^* = 1.5$.

CFD simulations were performed for the two design cases to validate the viability of the LESP concept for advancing or delaying LEV formation according to specification. Figure 26 shows vorticity plots for the baseline case and the two design cases, at several equally spaced intervals through the respective motions. The

plots confirm that LEV formation can indeed be advanced (as in design1 to $t^* = 0.5$) or delayed (as in design2 in to $t^* = 1.5$) by suitably by superimposing a suitable plunge motion. Using the LESP concept and calculating suitable superpositions, LEV formation for any arbitrary motion may be triggered at will or suppressed entirely.

5 Conclusions

In this paper, an inviscid theoretical method which handles large amplitudes and nonplanar wakes is presented, and used to derive the leading-edge suction parameter (LESP) which is a measure of the suction at the airfoil leading edge. Parametric studies with experiments and CFD are used to rigorously test the LESP hypothesis, that there is a motion-independent critical value of the LESP for a given airfoil and Reynolds number at which LEV formation is initiated.

In conclusion, it was seen that there is a critical value of the LESP for a given airfoil and Reynolds number at which LEV formation is initiated, except for motions with varying pitch rates that have varying degrees of trailing-edge flow separation. The value of critical LESP is seen to be independent of kinematic parameters such as amplitude, pivot location and type of motion (pitch/plunge). For kinematics with varying pitch rates, the critical LESP is observed to increase with increasing pitch rates. This behavior is likely related to the different degrees of trailing-edge boundary-layer separation for these cases which is not modeled in the current research, although this needs to be confirmed with further investigations. Hence, the use of LESP must be restricted to kinematics with high pitch rates ($K > 0.1$), well beyond those typical of dynamic stall, where the influence of trailing-edge separation is comparatively small. In this regime, by pre-determining the critical LESP for a given airfoil and Reynolds number, it is possible to predict whether LEVs will be formed for any given motion kinematics. Further, the LESP may be used in a design approach to generate motion kinematics which would either prevent LEV formation or generate LEVs as per aerodynamic requirements. The results demonstrate that the LESP is a fundamentally important, albeit simple, theoretical parameter that governs LEV formations. This use of this concept is not restricted to the thin-airfoil formulation presented in this paper, and may be employed to augment any unsteady panel method or potential flow solver to predict and model LEV formation and shedding in fast-rate kinematics.

Acknowledgements The authors wish to gratefully acknowledge the support of the U.S. Air Force Office of Scientific Research through Grant FA 9550-13-1-0179; Program manager: Dr. Douglas Smith.

References

1. Abbott, I.H., von Doenhoff, A.E.: Theory of Wing Sections. Dover, New York (1959)
2. Acharya, M., Metwally, M.H.: Unsteady pressure field and vorticity production over a pitching airfoil. AIAA J. **30**(2), 403–411 (1992)
3. Baik, Y.S., Bernal, L.P., Granlund, K., Ol, M.V.: Unsteady force generation and vortex dynamics of pitching and plunging aerofoils. J. Fluid Mech. **709**(1), 37–68 (2012). doi:10.1017/jfm.2012.318
4. Beddoes, T.S.: Onset of leading edge separation effects under dynamic conditions and low Mach number. In: 34th Annual forum of the American Helicopter Society (1978)
5. Bos, F.M., van Oudheusden, B.W., Bijl, H.: Wing performance and 3-D vortical structure formation in flapping flight. J. Fluids Struct. **42**, 130–151 (2013)
6. Brunton, S.L., Rowley, C.W., Williams, D.R.: Reduced-order unsteady aerodynamic models at low Reynolds numbers. J. Fluid Mech. **724**(1), 203–233 (2013)
7. Carr, L.: Progress in analysis and prediction of dynamic stall. J. Aircr. **25**(1), 6–17 (1988)
8. Carr, L.W., Platzer, M.F., Chandrasekhara, M.S., Ekaterinaris, J.: Experimental and computational studies of dynamic stall. In: Cebeci, T. (ed.) Numerical and Physical Aspects of Aerodynamic Flows IV, pp. 239–256. Springer, Berlin (1990). doi:10.1007/978-3-662-02643-4_15
9. Carr, Z.R., Chen, C., Ringuette, M.J.: Finite-span rotating wings: three-dimensional vortex formation and variations with aspect ratio. Exp. Fluids **54**(2), 1–26 (2013)
10. Cassidy, D.A., Edwards, J.R., Tian, M.: An investigation of interface-sharpening schemes for multi-phase mixture flows. J. Comput. Phys. **228**(16), 5628–5649 (2009). doi:10.1016/j.jcp.2009.02.028
11. Chandrasekhara, M.S., Ahmed, S., Carr, L.W.: Schlieren studies of compressibility effects on dynamic stall of transiently pitching airfoils. J. Aircr. **30**(2), 213–220 (1993). doi:10.2514/3.48268

12. Choi, J.I., Edwards, J.R.: Large eddy simulation and zonal modeling of human-induced contaminant transport. Indoor Air **18**(3), 233–249 (2008)
13. Choi, J.I., Edwards, J.R.: Large-eddy simulation of human-induced contaminant transport in room compartments. Indoor Air **22**(1), 77–87 (2012)
14. Choi, J.I., Oberoi, R.C., Edwards, J.R., Rosati, J.A.: An immersed boundary method for complex incompressible flows. J. Comput. Phys. **224**(2), 757–784 (2007)
15. DeVoria, A.C., Ringuette, M.J.: Vortex formation and saturation for low-aspect-ratio rotating flat-plate fins. Exp. Fluids **52**(2), 441–462 (2012)
16. Dickinson, M.H., Gotz, K.G.: Unsteady aerodynamic performance of model wings at low Reynolds numbers. J. Exp. Biol. **174**(1), 45–64 (1993)
17. Doligalski, T.L., Smith, C.R., Walker, J.D.A.: Vortex interactions with walls. Annu. Rev. Fluid Mech. **26**(1), 573–616 (1994)
18. Edwards, J.R., Chandra, S.: Comparison of eddy viscosity—transport turbulence models for three-dimensional, shock-separated flow fields. AIAA J. **34**(4), 756–763 (1996)
19. Ekaterinaris, J.A., Platzer, M.F.: Computational prediction of airfoil dynamic stall. Prog. Aerosp. Sci. **33**(11), 759–846 (1998)
20. Eldredge, J.D., Wang, C., Ol, M.V.: A computational study of a canonical pitch-up, pitch-down wing maneuver. In: AIAA Paper 2009-3687 (2009)
21. Ellington, C.P.: The novel aerodynamics of insect flight: applications to micro-air vehicles. J. Exp. Biol. **202**(23), 3439–3448 (1999)
22. Ellington, C.P., van den Berg, C., Willmott, A.P., Thomas, A.L.R.: Leading-edge vortices in insect flight. Nature **384**(1), 626–630 (1996)
23. Evans, W.T., Mort, K.W.: Analysis of computed flow parameters for a set of sudden stalls in low speed two-dimensional flow. NACA Report TN D-85 (1959)
24. Fage, A., Johansen, F.C.: On the flow of air behind an inclined flat plate of infinite span. In: Proceedings of the Royal Society of London. Series A, Containing Papers of a Mathematical and Physical Character, Vol. 116(773), pp. 170–197 (1927)
25. Garmann, D.J., Visbal, M.R.: Numerical investigation of transitional flow over a rapidly pitching plate. Phys. Fluids **23**, 094,106 (2011)
26. Garrick, I.E.: Propulsion of a flapping and oscillating airfoil. NACA Report, p. 567 (1937)
27. Ghosh Choudhuri, P., Knight, D., Visbal, M.R.: Two-dimensional unsteady leading-edge separation on a pitching airfoil. AIAA J. **32**(4), 673–681 (1994)
28. Granlund, K., Ol, M.V., Bernal, L.: Experiments on pitching plates : force and flowfield measurements at low Reynolds numbers. In: AIAA Paper 2011-0872 (2011)
29. Granlund, K., Ol, M.V., Bernal, L.P.: Unsteady pitching flat plates. J. Fluid Mech. **733**(1), R5 (2013)
30. Hemati, M.S., Eldredge, J.D., Speyer, J.L.: Improving vortex models via optimal control theory. J. Fluids Struct. **49**, 91–111 (2014)
31. Jantzen, R.T., Taira, K., Granlund, K., Ol, M.V.: Vortex dynamics around pitching plates. Phys. Fluids **26**(5), 053,606 (2014)
32. Jones, A.R., Babinsky, H.: Unsteady lift generation on rotating wings at low Reynolds numbers. J. Aircr. **47**(3), 1013–1021 (2010)
33. Jones, A.R., Babinsky, H.: Reynolds number effects on leading edge vortex development on a waving wing. Exp. Fluids **51**(1), 197–210 (2011)
34. Jones, K.D., Platzer, M.F.: A fast method for the prediction of dynamic stall onset on turbomachinery blades. In: ASME Paper 97-GT-101 (1997)
35. Jones, W.P.: Aerofoil oscillations at high mean incidences. A.R.C. Report 2654 (1953)
36. von Kármán, T., Burgers, J.M.: General aerodynamic theory-perfect fluids. In: Durand, W.F. (ed.) Aerodynamic Theory: A General Review of Progress, vol. 2. Dover Publications, Mineola (1963)
37. Katz, J.: Discrete vortex method for the non-steady separated flow over an airfoil. J. Fluid Mech. **102**(1), 315–328 (1981)
38. Katz, J., Plotkin, A.: Low-Speed Aerodynamics, Cambridge Aerospace Series. Cambridge University Press, Cambridge (2000)
39. Koochesfahani, M.M., Smiljanovski, V.: Initial acceleration effects on flow evolution around airfoils pitching to high angles of attack. AIAA J. **31**(8), 1529–1531 (1993)
40. Leishman, J.G.: Principles of Helicopter Aerodynamics, Cambridge Aerospace Series. Cambridge University Press, Cambridge (2002)
41. Leishman, J.G., Beddoes, T.S.: A semi-empirical model for dynamic stall. J. Am. Helicopter Soc. **34**(3), 3–17 (1989)
42. McAvoy, C.W., Gopalarathnam, A.: Automated cruise flap for airfoil drag reduction over a large lift range. J. Aircr. **39**(6), 981–988 (2002)
43. McCroskey, W.: The phenomenon of dynamic stall. NASA Technical Memorandum (81264) (1981)
44. McCroskey, W.J.: The Phenomenon of Dynamic Stall. NASA TM 81264 (1981)
45. McCroskey, W.J.: Unsteady Airfoils. Annu. Rev. Fluid Mech. **14**, 285–311 (1982)
46. McGowan, G.Z., Granlund, K., Ol, M.V., Gopalarathnam, A., Edwards, J.R.: Investigations of lift-based pitch-plunge equivalence for airfoils at low Reynolds numbers. AIAA J. **49**(7), 1511–1524 (2011)
47. Morris, W.J., Rusak, Z.: Stall onset on aerofoils a low to moderately high Reynolds number flows. J. Fluid Mech. **733**(1), 439–472 (2013)
48. Mueller, T.J. (ed.): Fixed and Flapping Wing Aerodynamics for Micro Air Vehicle Applications, Progress in Astronautics and Aeronautics, vol. 195. AIAA Inc., Virginia (2001)
49. Ol, M.V.: Unsteady low Reynolds number aerodynamics for micro air vehicles (MAVS). DTIC Document AFRL-V A-WP-TM-2007-3080 (2007)
50. Ol, M.V., Bernal, L., Kang, C.K., Shyy, W.: Shallow and deep dynamic stall for flapping low Reynolds number airfoils. Exp. Fluids **46**(5), 883–901 (2009)
51. Ol, M.V., McAuliffe, B.R., Hanff, E.S., Scholz, U., Kaehler, C.: Comparison of laminar separation bubble measurements on a low Reynolds number airfoil in three facilities. In: AIAA Paper 2005-5149 (2005)

52. Ol, M.V., Reeder, M., Fredberg, D., McGowan, G.Z., Gopalarathnam, A., Edwards, J.R.: Computation versus experiment for high-frequency low-Reynolds number airfoil plunge. Int. J. Micro Air Veh. **1**(2), 99–119 (2009)
53. Panah, A.E., Akkala, J.M., Buchholz, J.H.J.: Vorticity transport and the leading-edge vortex of a plunging airfoil. Exp. Fluids **56**(8), 1–15 (2015)
54. Pinkerton, R.B.: Calculated and measured pressure distribution over the midspan section of the NACA 4412 airfoil. NACA Report 563 (1936)
55. Pitt Ford, C.W., Babinsky, H.: Lift and the leading-edge vortex. J. Fluid Mech. **720**(1), 280–313 (2013)
56. Polhamus, E.C.: A concept of the vortex lift of sharp-edge delta wings based on a leading-edge-suction analogy. NASA TN D-3767 (1966)
57. Ramesh, K., Gopalarathnam, A., Edwards, J.R., Ol, M.V., Granlund, K.: An unsteady airfoil theory applied to pitching motions validated against experiment and computation. Theor. Comput. Fluid Dyn. **27**(6), 843–864 (2013)
58. Ramesh, K., Gopalarathnam, A., Granlund, K., Ol, M.V., Edwards, J.R.: Discrete-vortex method with novel shedding criterion for unsteady airfoil flows with intermittent leading-edge vortex shedding. J. Fluid Mech. **751**, 500–538 (2014)
59. Ramesh, K., Gopalarathnam, A., Ol, M.V., Granlund, K., Edwards, J.R.: Augmentation of inviscid airfoil theory to predict and model 2D unsteady vortex dominated flows. AIAA Paper 2011-3578 (2011)
60. Ramesh, K., Murua, J., Gopalarathnam, A.: Limit-cycle oscillations in unsteady flows dominated by intermittent leading-edge vortex shedding. J. Fluids Struct. **55**, 84–105 (2015)
61. Rival, D., Prangemeier, T., Tropea, C.: The influence of airfoil kinematics on the formation of leading-edge vortices in bio-inspired flight. Exp. Fluids **46**(5), 823–833 (2009)
62. Sarpkaya, T.: An inviscid model of two-dimensional vortex shedding for transient and asymptotically steady separated flow over an inclined plate. J. Fluid Mech. **68**(01), 109–128 (1975)
63. Sears, W.R.: Some recent developments in airfoil theory. J. Aeronaut. Sci. **23**(1), 490–499 (1956)
64. Selig, M.S., Lyon, C.A., Giguere, P., Ninham, C., Guglielmo, J.J.: Summary of Low-Speed Airfoil Data, vol. 2. SoarTech Publications, Virginia Beach, VA (1995)
65. Shyy, W., Liu, H.: Flapping wings and aerodynamic lift: the role of leading-edge vortices. AIAA J. **45**(12), 2817–2819 (2007)
66. Spalart, P.R., Allmaras, S.R.: A one-equation turbulence model for aerodynamic flows. AIAA Paper 92-0439 (1992)
67. Taha, H.E., Hajj, M.R., Beran, P.S.: State-space representation of the unsteady aerodynamics of flapping flight. Aerosp. Sci. Technol. **34**, 1–11 (2014)
68. Theodorsen, T.: On the theory of wing sections with particular reference to the lift distribution. NASA TR 383 (1931)
69. Theodorsen, T.: General theory of aerodynamic instability and the mechanism of flutter. NACA Report 496 (1935)
70. Visbal, M.R., Gordnier, R.E., Galbraith, M.C.: High-fidelity simulations of moving and flexible airfoils at low Reynolds numbers. Exp. Fluids **46**(5), 903–922 (2009)
71. Visbal, M.R., Shang, J.S.: Investigation of the flow structure around a rapidly pitching airfoil. AIAA J. **27**(8), 1044–1051 (1989)
72. Visbal, M.R., Yilmaz, T.O., Rockwell, D.: Three-dimensional vortex formation on a heaving low-aspect-ratio wing: computations and experiments. J. Fluids Struct. **38**, 58–76 (2013)
73. Wagner, H.: Über die Entstehung des dynamischen Auftriebes von Tragflügeln. ZaMM **5**(1), 17–35 (1925)
74. Wang, C., Eldredge, J.D.: Low-order phenomenological modeling of leading-edge vortex formation. Theor. Comput. Fluid Dyn. **27**(5), 577–598 (2012)
75. Widmann, A., Tropea, C.: Parameters influencing vortex growth and detachment on unsteady aerodynamic profiles. J. Fluid Mech. **773**, 432–459 (2015)
76. Woods, L.C.: The lift and moment acting on a thick aerofoil in unsteady motion. Philos. Trans. R. Soc. Lond. A Math. Phys. Eng. Sci. **247**(925), 131–162 (1954)